Reference seismic crustal model of the Dinarides

Katarina Zailac[1], Bojan Matoš[2], Igor Vlahović[2], Josip Stipčević[3]

5   1 University of Zagreb University Computing Centre - SRCE, Zagreb, 10000, Croatia
2 Faculty of Mining, Geology and Petroleum Engineering, University of Zagreb, Zagreb, 10000, Croatia
3 Department of Geophysics, Faculty of Science, University of Zagreb, Zagreb, 10000, Croatia

Correspondence: Josip Stipčević (jstipcevic.geof@pmf.hr)

10

Abstract

Continental collision zones are structurally one of the most heterogeneous areas intermixing various different units within a relatively small space. A good example of this is the Dinarides, a mountain chain situated in the central Mediterranean, where thick carbonates cover older

15   crystalline basement units and remnants of subducted oceanic crust. This is further complicated by the highly variable crustal thickness ranging from 20 to almost 50 km. In terms of spatial extension, this area is relatively small, but covers tectonically differentiated domains making any seismic or geological analysis complex, with significant challenges in areas that lack seismic information on crustal structure.

20   Presently there is no comprehensive 3-D crustal model of the Dinarides (and surrounding areas). Using the compilations of previous studies and employing kriging interpolation, we created a vertically and laterally varying crustal model defined on a regular grid for the wider area of the Dinarides, also covering parts of Adriatic Sea and the SW part of the Pannonian Basin. The model is divided by three interfaces, Neogene deposits bottom, Carbonate rock

25   complex bottom and Moho discontinuity, with seismic velocities (P- and S-) and density defined at each grid point. To validate the newly derived model, we calculated travel times for an earthquake recorded on several seismic stations in the Dinarides area. The calculated travel times show significant improvement when compared to the simple 1D model used for routine earthquake location in Croatia.

30   The model derived in this work represents the first step towards improving our knowledge of the crustal structure in the complex area of the Dinarides. We hope that the newly assembled model will be useful for all forthcoming studies (e.g. as a starting model for seismic tomography, as a model for earthquake simulations) which require knowledge of the crustal structure.

35   Introduction

The first seismic investigation done in the wider Dinarides region can be traced to Mohorovičić's famous discovery of the boundary between Earth's crust and mantle

(Mohorovičić, 1910). The earliest deep seismic sounding experiments investigating the crustal structure beneath the Dinarides were conducted in the 1960s (Dragašević and Andrić, 1975; Aljinović, 1983; Aljinović et al., 1987). The most important results from those early investigations were about the thickness of the upper crust (Aljinović, 1983). In more recent times, there was another set of active seismic experiments. The ALP 2002 (Brückl et al., 2007) focused on the investigation of the Eastern Alps but also covered the northernmost part of the Dinarides and the Panonnian basin. As part of the same international experiment, Šumanovac et al. (2009) modeled velocities in the crust and uppermost mantle from the measurements taken along the Alp07 profile located at the crossing between NW Dinarides and SW margin of the Pannonian basin. The results from the Alp07 profile were later extended by several studies including gravimetric modeling, P-wave receiver function analysis and local earthquake tomography (Šumanovac, 2010; Šumanovac et al., 2016; Orešković et al., 2011; Kapuralić et al., 2019), covering only the NW part of the Dinarides and SW part of the Pannonian basin. These studies reported a two-layer crust in the area of the Dinarides, and one-layer crust in the area of the Pannonian basin.

The first Moho map of the Dinarides was compiled by Skoko et al. (1987) utilizing gravimetric data from that area. Similarly, Šumanovac (2010) used results from active seismic experiments (Alp07) to calibrate gravimetric data and get a more accurate map of Moho depths in the region. Stipčević et al. (2011) were first to use direct seismic measurements in the central and southern Dinarides, extending the analysis of Moho depths to that region. For this, they employed the P-wave receiver functions (PRF) method and by modeling it found an intra-crustal reflector in the area of the Internal Dinarides. Stipčević et al. (2020) extended the PRF analysis by including significantly more stations and created the map of Moho depths beneath the Dinarides. In that expanded receiver function study, Stipčević et al. (2020) report significantly thicker crust in the area of the southern Dinarides compared to the previous studies.

Complementary to the crustal exploration there have also been some recent investigations of the uppermost mantle. Using the S-wave receiver functions (SRF) Belinić et al. (2018) mapped the lithosphere–asthenosphere boundary (LAB) under the Dinarides. The most interesting feature of that LAB map is the lack of deep lithospheric root beneath the central Dinarides, which was interpreted as thinning of the lithosphere due to possible lithospheric mantle delamination. Two years later, there was a complementary study by Belinić et al. (2020), using Rayleigh wave tomography in order to obtain an upper mantle S-wave velocity model for the greater Dinarides area. Similar to their first work, authors reported a missing deep lithospheric root in the area of the central Dinarides, and a high velocity uppermost mantle anomaly visible in the southern Dinarides.

From this short outline of the main geophysical investigations done in the wider Dinarides area it is obvious that the crustal structure of the region is fairly complex with quite a long

history of geophysical exploration. Despite this, there has never been an attempt (as far as we know) to combine these results in order to create an extensive regional 3-D crustal model for the Dinarides. The area was covered by the global and continental scale models, but the authors of these studies pointed out the lack of available data in the Dinarides area (e.g., Grad et al. 2009, Molinari and Morelli 2011, Artemieva et al., 2013). Note that those continental scale models were published prior to some of the investigations whose results were used for derivation of our crustal model. Regional scale crustal models are an important factor in all seismic studies relying on waveform modeling and seismic wave traveltime inversion. This is especially exacerbated in areas with complex crustal structure such as the Dinarides. Therefore, it is necessary to assemble a comprehensive, ready-to-use model based on all the available results.

In this study we focus on the crust and include all the data regarding crustal structure available to us, into a 3-D model covering the area of the Dinarides. The aim is to create a vertically and laterally varying crustal model defined on a regular grid for the wider area of the Dinarides. This model will be a good starting point for both body and surface wave tomography studies and provide an excellent base model for local and regional physics-based earthquake shaking scenarios. Besides the seismic velocity as the main parameter describing the crustal structure, we also include existing data on the Moho discontinuity depth, and the approximate thickness of a carbonate rock layer (the Carbonate rock complex, CRC) in the Dinarides. Even though our crustal model is focused on the Dinarides, part of it also covers the SW margin of the Pannonian basin and Adriatic Sea (Fig. 1).

Tectonic and geological setting

The Alpine–Carpathian–Dinaridic–Albanide–Hellenic orogenic system is a part of a Circum-Mediterranean orogenic system. Encircling the Neogene Pannonian Basin System (PBS), this orogenic system is constructed of tectonostratigraphic units derived from both the Adriatic microplate and the European plate that were separated by the Neotethyan Ocean (Schmid et al., 2008, 2020, and references therein). Tectonic units were amalgamated by fold-and-thrust systems of different polarity facing either the European foreland (e.g., Western and Eastern Alps, and Carpathians) or the Adriatic foreland (e.g., Southern Alps, Dinarides, Albanides, Hellenides) as a result of a change in subduction polarity between the European plate and the Adriatic Microplate (Schmid et al., 2008, 2020; Ustaszewski et al., 2008).

The tectonic evolution of these large orogenic systems, i.e., Dinarides *sensu lato*, started with the Triassic (c. 220 Ma) opening of the Neotethys oceanic embayment between the African and Eurasian Plates. The Neotethys Ocean continued spreading during Late Triassic and Early to Mid-Jurassic, being interrupted only by intra-oceanic subduction of the Western Vardar oceanic domain and ophiolite obduction onto the eastern margin of the Adriatic

Microplate (see Schmid et al., 2020 for details). According to Schmid et al. (2008), the Neotethys Ocean, i.e., the Eastern Vardar oceanic domain remained open through the Late Jurassic–Cretaceous period (see Ustaszewski et al., 2009 and references therein).

115   The final closure of the Neotethys oceanic realm coincided with the collision of the Adria Microplate and the European foreland during the Late Cretaceous–Early Paleogene (Schmid et al., 2020 and references therein) that initiated formation of the Dinarides (Środoń et al., 2018). During the Middle Eocene–Oligocene, the regional NE–SW oriented compression caused NE-directed continental subduction and formation of complex fold-and-thrust sheets
120   in the Dinaridic region due to SW-directed thrusting of Adria derived units, whereas in the internal Dinaridic domains, E–W oriented compression caused the formation of the W-directed thrusting of the Tisza Mega-Unit over the Internal parts of the Dinarides (e.g., Handy et al., 2019; Schmid et al., 2020; Balling et al., 2021 and references therein). Continuous convergence of the Adria indenter towards the European foreland in the Late Oligocene–
125   Early Miocene further contributed to nappe stacking and thrusting in the Alps and Dinarides, but it also accommodated c. 400 km of E-directed orogen-parallel lateral extrusion of the ALCAPA block (including the Eastern Alps, West Carpathians and Transdanubian ranges north of the Lake Balaton) and active "back-arc-type" extension in the PBS (Royden and Horváth, 1988; Ratschbacher et al., 1991a, b; Frisch et al., 1998; Fodor et al., 1998; Tari et al.,
130   1999; Csontos and Vörös, 2004; Horváth et al. 2006; Cloetingh et al., 2006; Schmid et al., 2008).

With an area of 80–200 km wide and nearly 700 km long, the Dinarides are a fold-and-thrust orogenic belt constructed from thrust sheets divided into internal and external tectonic domains (see **Fig. 1**). The lithological succession in the Internal Dinarides is characterized
135   by units that comprise passive margin ophiolitic successions and pelagic derived sedimentary rocks, while the External Dinarides are dominated mainly by shallow marine carbonate platform deposits that in places reach 8000 m of thickness (Vlahović et al., 2005). Due to paleogeographic differences and tectonic complexity, the Dinaridic lithological succession is spatially highly varied in its thickness and exposure (Vlahović et al., 2005,
140   Schmid et al., 2020; Balling et al., 2021).

The oldest rocks cropping out in the External Dinarides are Carboniferous to Middle Triassic siliciclastic–carbonate deposits accumulated along the Gondwanian passive continental margin, which due to regional extensional tectonics marked by Middle Triassic volcanism differentiated the area, thus forming isolated shallow marine carbonate platforms (Vlahović
145   et al., 2005). Through the Middle Triassic–Cretaceous timespan, carbonate platforms in the region were surrounded by deeper marine areas and characterized by mostly continuous shallow-marine carbonate deposition, though the last extensional phase in Toarcian resulted in a disintegration in several smaller platforms, including the Adriatic Carbonate Platform, Apenninic Carbonate Platform and Apulian Carbonate Platform (Vlahović et al., 2005 and

references therein). During the 120 My of existence of the Adriatic Carbonate Platform (AdCP), i.e., from Early Jurassic to Late Cretaceous (locally even to early Paleocene – Tešović et al., 2020), the thickness of deposited carbonate successions reached between 3500 and 5000 m (Vlahović et al., 2005 and references therein). The AdCP deposition ended due to regional emergence in the Late Cretaceous–Paleogene, which was linked and enhanced by tectonic deformations and continent collision of the Adria Microplate and the European foreland yielding deposition of synorogenic turbiditic deposits ("flysch") in newly formed foreland basins (Vlahović et al., 2005; Schmid et al., 2008 and references therein). The final uplift of the Dinarides took place from the Middle Eocene to Oligocene (Dinaric phase; see Schmid et al., 2008; Balling et al., 2021 with references).

Modeling approach

Generally, the new model is defined as a one-layered crust with laterally and vertically variable parameters (seismic velocities and density). This was done due to the fact that only information about crustal thickness was available for the whole investigated region Nevertheless, during data collection and integration within the new model we realized that the Neogene deposits in the Pannonian Basin make up a very thick and distinct layer, and just incorporating it into a one-layered model would be an oversimplification. In the light of the Pannonian basin sedimentary complex being significantly different from the rest of the crust, we included a Neogene deposits layer on top of a laterally and vertically varying crust. The same goes for the Paleozoic-Paleogene carbonates in the Adriatic–Dinarides region as there are numerous studies indicating distinct reflections from the bottom of the CRC in the seismic reflection studies (Dragašević and Andrić, 1975; Aljinović, 1983; Aljinović et al., 1987). Given that there was no data on any of the parameters in this layer (velocity or density), we only included the CRC bottom depth in our model. The velocity and density of the CRC were not interpolated separately but were interpolated using the same input velocity (and density) data we had available for the rest of the crust. This choice seems reasonable, since each of the profiles used crosses the part of the investigated area covered with carbonates, and samples its features, even though none of the studies used explicitly interpreted carbonates as a separate layer.

To compile the data for the new crustal model, we used all available and published results on seismic and geologic structure of the crust and uppermost mantle. Some of them were not available in a digital form (mostly the studies published before 2010) and had to be digitized manually. The datasets used are very diverse: two 3-D crustal models (one consisting of a two-layered crust with interface depth information while the other had a single-layered crust), several 2D interface maps (Moho depths and Neogene deposits maps), three seismic refraction/wide angle reflection profiles (which were the basic source for velocity data) and five gravimetric profiles. Coverage of the datasets used to compile the 3-D crustal model of

the Dinarides is shown in **Fig. 1.** and details are listed in **Table 1**. The exact locations of data points used are shown in Appendix B.
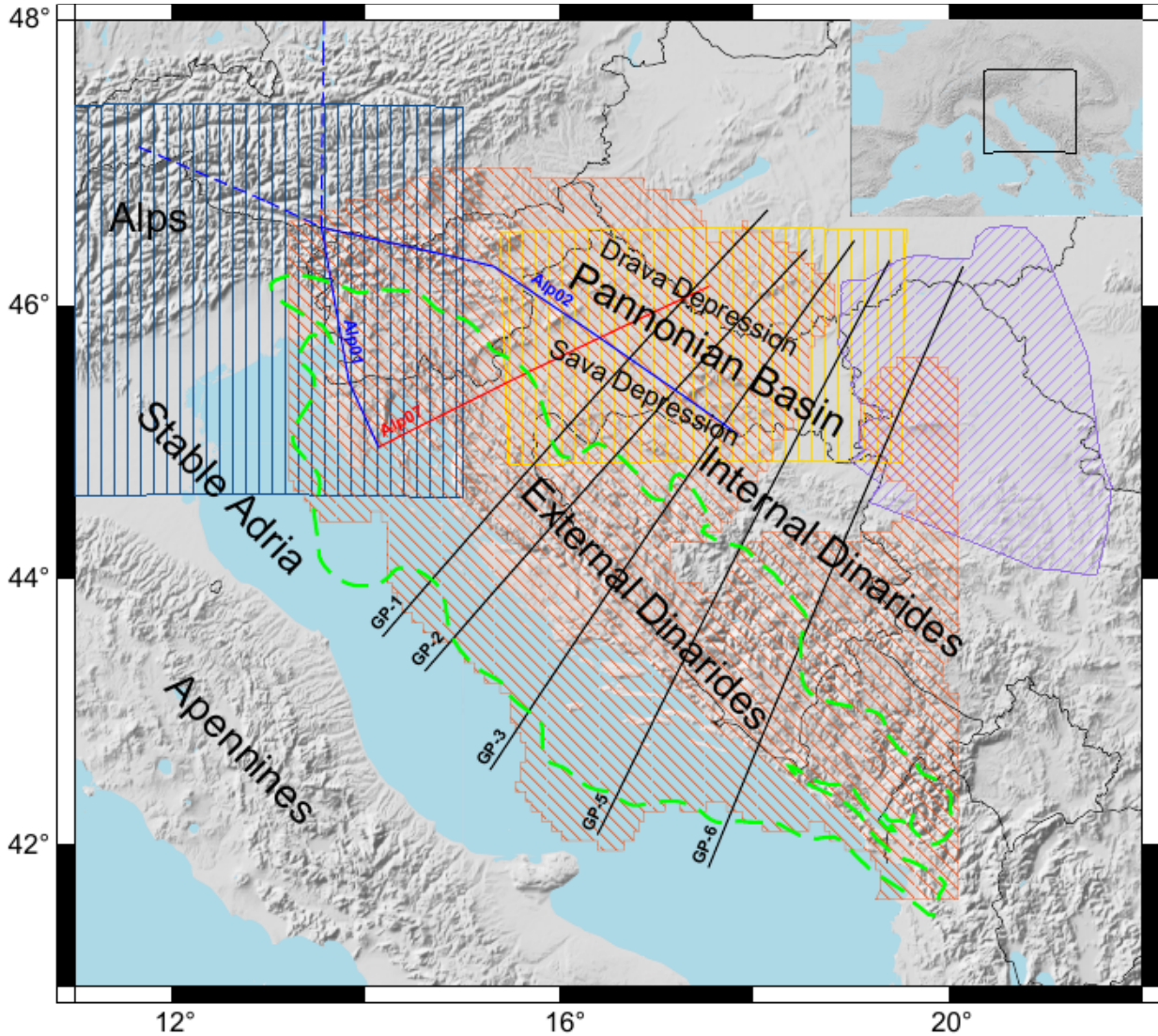
Figure 1. Compilation of data used in this study. Blue lines mark the positions of Alp01 and Alp02 profiles (Brückl et al., 2007) – only the full line parts are used in the study; the red line is the position of the Alp07 profile (Šumanovac et al., 2009); black lines are the positions of gravimetric profiles GP-1 to GP-6 (Šumanovac, 2010). Orange shaded area shows Moho depth data coverage from the receiver function study of Stipčević et al. (2020), blue vertically shaded area is the NAC model (Magrin and Rossi, 2020). The yellow shaded area shows the extent of Saftić et al. (2003) data on the Pannonian basin Neogene deposits, and the purple shaded area shows the extent of data on the Pannonian basin Neogene deposits from Matenco and Radivojević (2012). Green dashed line marks the extension of the AdCP carbonate rocks from Tišljar et al. (2002). The sources of the data shown in this map are listed in **Table 1**.

Table 1. List of the data sources used for the Dinarides crustal model.

Profile, model, or project name	Data type	Reference	Processing	Results type
Alp01 and Alp02	Seismic refraction and wide angle reflection	Brückl et al. (2007)	profiles manually digitized	Vp, Moho
Alp07	Seismic refraction and wide angle reflection	Šumanovac et al. (2009)	profile manually digitized	Vp, Moho
GP-1, GP-2, GP-3, GP-5, GP-6	2D gravity modeling	Šumanovac (2010)	profiles manually digitized	Vp, density, Moho
	Receiver functions	Stipčević et al. (2020)	available in digital form	Moho
The Northern Adria Crust (NAC) model	Multiple data sets	Magrin and Rossi (2020)	available in digital form	Vp, density, Moho
	Isopach map	Saftić et al. (2003)	digitized manually	Neogene deposits bottom depth
	Multiple data sets	Matenco and Radivojević (2012)	digitized manually	Neogene deposits bottom depth
	Carbonate rock complex distribution	Tišljar et al. (2002)	digitized manually	CRC bottom depth

	Geological map	Basic Geological Map (1:100,000) of former Yugoslavia (Osnovna Geološka Karta SFRJ)	digitized manually	CRC bottom depth
	Geological map	1:200,000 Geological Map of Albania (Geological Map of Albania, 2002)	digitized manually	CRC bottom depth
	Constructed and balanced geological cross-sections	Balling et al., (2021)		CRC bottom depth
EPcrust		Molinari and Morelli (2011)	available in digital form	Vp, Moho
SRTM15+V2.0	Global elevation grid	Tozer et al. (2019)	available in digital form	Topography

205 The interpolation of model parameters was done using kriging method (for details see Appendix C), which is formulated for the estimation of a continuous spatial attributes (e.g. depth to Moho interface) at an unknown site, using the limited set of data from sampled sites. Since kriging requires Cartesian coordinates, we transformed the data to ETRS89-extended/LAEA Europe Cartesian coordinate system (Annoni et al., 2003), which is defined

210 on the entire investigated area. The transformations were done using the *pyproj* package (Snow et al. 2021). Kriging interpolation was done using the *gstat* package (Pebesma, 2004). Interface data were interpolated on a regular 5 km × 5 km grid, and the velocity and density were interpolated on a slightly more complex grid: the horizontal grid is the same as for the interfaces (5 km × 5 km), but the vertical spacing changes with depth (in the first 10 km of

215 depth, the spacing is 0.5 km; between depths of 10 km and 20 km, vertical spacing is 1 km, and at greater depths, vertical spacing is 2.5 km). This scheme was used to account for better sampling and more heterogeneous upper crust.

Initially, we specified a relatively large area between 10° and 22° east longitude and 39° and 48° north latitude as the starting region of investigation. We performed interpolation in the entire initial region for each interface separately. As some of the areas in the initial region were not covered by data points (see Appendix B) the final model area was reduced based on the Moho discontinuity depth errors in combination with lower uncertainty areas of the Vp model. The final model covers, roughly, the area between 13° E and 20° E, and 42° N and 47° N.

Kriging does not allow multiple values at a single point in space (i.e. there is no overlapping), so all overlapping data from various sources was processed before the interpolation. We tried to reduce subjectivity as much as possible, and therefore included known and estimated variances into the data processing. In case of the data overlapping, we calculated the value which was used for interpolation (depth for interfaces or velocity/density for layer parameters) at the given point as a weighted mean of multiple values from different sources, with inverse of variances used as weights:

$$\hat{d}_m = \frac{\sum_i \frac{1}{\sigma_i^2} d_{m,i}}{\sum_i \frac{1}{\sigma_i^2}},$$

where $d_{m,i}$ is the value at point i, and σ_i^2 is variance at point i.

We also included error estimates in the final model. To calculate the total error of the model, we followed the procedure applied by Magrin and Rossi (2020) for the derivation of the NAC model. With the assumption of Gaussian distribution of errors, the total variance of the model is the sum of two terms: the variance of the input data, and the variance from the interpolation itself. The interpolation variance term was provided by the *gstat* package along with the interpolated data. In order to calculate the variance at each grid point, we interpolated the input data variances on the same grid as the data itself.

There are four interfaces defined in the presented model – CRC bottom, Neogene deposits bottom, Mohorovičić discontinuity (Moho), and topography/bathymetry. It should be noted that Neogene and CRC bottom depths are not defined for all locations in the model. The model parameters (seismic velocities and density) are defined on a regular grid and were calculated differently for the Neogene deposits layer and the rest of the crust.

The information about the Moho depth was compiled from a large number of available studies. The main source of Moho data was the receiver function (RF) study of Stipčević et al. (2020). These results are digitally available as the crustal thickness map on a regular 8.3 km × 8.3 km grid (location shown in **Fig. 1**), and it includes error estimates on the same grid. We also included Moho data from seismic refraction and wide angle reflection profiles

(Brückl et al., 2007; Šumanovac et al., 2009; profiles' locations shown in **Fig. 1**), and from the gravimetric profiles (Šumanovac, 2010; **Fig. 1**). All profiles (both seismic and gravimetric) are available as figures in digital form, but depth information had to be digitized manually. Each profile was first georeferenced, and the interpreted Moho depths were digitized every 5 km along the profile's length. For the profile data, there are no detailed error estimates but the authors report that the Moho interface was resolved to at least ±2–3 km for refraction and wide angle reflection profiles. As there are no such estimates for the gravimetric profiles and the reported errors are only general, we decided to include the error estimates as described in Grad et al. (2009). The authors had a similar problem while building the Moho model for the European continent but had much more input data to come up with reasonable error estimates. According to them, the error estimates for Moho obtained from the seismic profiles should be about 6% of the Moho depth. That estimate fits nicely within the error estimates reported by Brückl et al. (2007) and Šumanovac et al. (2009) for refraction and wide angle reflection profiles used in this study. As for error estimates in gravimetric profiles, we used the values from the study of Grad et al. (2009), which reported somewhat higher errors, of about 20% of the estimated depths. For the NW part of our model, the Moho data from the high-quality and digitally available Northern Adria Crust (NAC) model (Magrin and Rossi, 2020) was also included. NAC interfaces are defined on a regular ∼ 5 km × 5 km grid with error estimations on the same grid (location shown in **Fig. 1**).

The data for the Neogene deposits base depth came from several geological studies. Largest volumes of the study area covered with unconsolidated Neogene deposits are situated in the SW part of the Pannonian Basin. As the basis for the definition of the Neogene sedimentary cover thickness in this region we used data from Saftić et al. (2003), which covers the southernmost part of the Pannonian Basin (**Fig. 1**). While preparing the data, we encountered the problem that missing deposits depth information for the eastern part of our study area is causing artifacts on the border of our model after the interpolation. To mitigate this, we included data from the study by Matenco and Radivojević (2012). Neogene deposits depth maps from both studies were scanned and georeferenced isolines were digitized every 5 km. For the error estimation we again turned to the study of Grad et al. (2009), where they estimated that the error for Moho should be about 15% for manually digitized maps. Since there was no error estimate beforehand, we decided to use the same percentage for Neogene deposits depth estimate. For the NW part of the study area, we included deposits bottom information from the NAC model.

The area of the Dinarides does not contain a significant Neogene soft deposits cover and is mainly overlain by a thick layer of Paleozoic-Paleogene Carbonate rock complex (CRC). Therefore, for the area of the Dinarides, we used the CRC distribution described in studies of Tišljar et al. (2002) and Vlahović et al. (2005) and used it as a zero-Neogene deposits-thickness area, although there are locally some very restricted Neogene deposits formed

within few intramontane basins. Here, the CRC border was georeferenced and digitized
290   manually (green dashed line in **Fig. 1**).

The interface with the least data available to us was the Carbonate rock complex (CRC) bottom depth. The CRC bottom depth was modelled by combining geological and structural data published in the available Basic Geological Map (1:100,000) of former Yugoslavia (Osnovna Geološka Karta SFRJ) with accompanying Explanatory Notes that cover the entire
295   Dinaridic area, Geological Map of Albania at the 1:200,000 scale (Geological Map of Albania, 2002) as well as geological-structural data published in studies of Tišljar et al. (2002), Vlahović et al., (2005) and Balling et al., (2021) (see Table A1). Based on the collected data, we determined the spatial extent of the Paleozoic–Paleogene CRC. Assessment of CRC thickness was initially performed at each geological map, using thicknesses presented in
300   geological columns on each map. Derived values of CRC thickness were further considered in respect to the deformation styles and large-scale structural relations (e.g., Balling et al., 2021). Several regional carbonate nappe systems in the External Dinarides characterized by extensive folding and thrusting could reach combined stacking thicknesses up to 12000 m, but thicknesses are not evenly distributed spatially. Significant variability of the CRC total
305   thickness in the Dinarides is caused by a combination of (1) initial differences in thickness due to significant paleogeographic differences along the Adria Microplate passive margin, with a total thickness of the Adriatic Carbonate Platform and thick underlying and thin overlying carbonates being in the range of 4500–8000 m (Tišljar et al., 2002; Velić et al., 2002; Vlahović et al., 2005), (2) structural position of individual nappe systems in respect to
310   the active collision front, and (3) variable strain rates and stress orientations during the Cretaceous–Paleogene Adria–Europe collision. Nappe stacking systems in the central and southern parts of the External Dinarides, where CRC is the thickest, locally incorporate up to four thrust sheets composed of different segments of the entire carbonate succession.

As for the physical characteristics, P-wave velocities were extracted from seismic refraction
315   and wide angle reflection studies (Brückl et. al, 2007; Šumanovac et al., 2009), densities from gravimetric profiles (Šumanovac, 2010), and P- and S-wave velocities and densities from the NAC model (Magrin and Rossi, 2020). We consider P-wave velocities as the best defined layer property, since the number of data sources for this parameter is largest. As for the S-wave velocity, there was only data from the NAC model, which is just a border area of our model.
320   Therefore, we did not interpolate S-wave velocity separately, but estimated it from the P-wave model. The mantle velocity shown was not estimated as part of this model, but was taken from Belinić et al. (2020), by calculating it from the Vs model reported there using the standard P over S-velocity ratio for the upper mantle (Vp/Vs = 1.73).

The NAC model is defined on a regular grid and was easily included in our data set. The
325   interpreted seismic reflection and refraction profiles (Brückl et al., 2007; Šumanovac et al., 2009) were digitized manually on a regular grid with the horizontal spacing of 5 km (along

the length of each profile) and vertical spacing of 1 km. Since the gravimetric profiles are interpreted in terms of homogeneous layers (density in a layer does not change vertically nor horizontally), we applied a slightly different logic. We used 5 km spacing along the profile and instead of regularly digitizing the densities in depth, we only picked one point in the middle of each layer representing the entire layer (see **Fig. 2**).
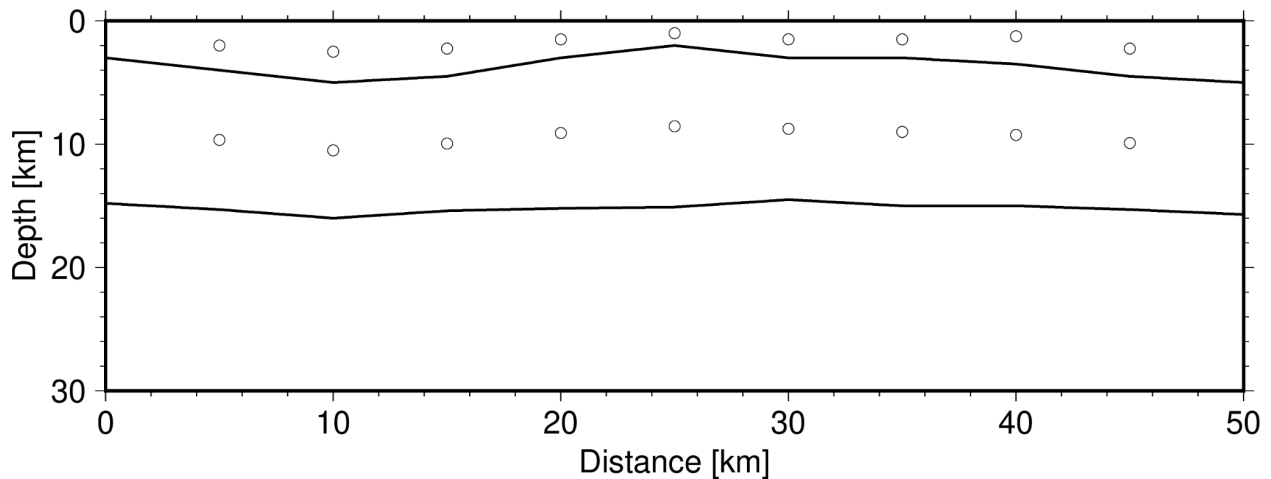

Figure 2. Simplified example of data sampling from one the gravimetric profiles with two interpreted layers. The dots represent digitized data points used to build our model. See text for details.

The NAC model (Magrin and Rossi, 2020) had reported parameter errors for each grid point and for interfaces, so these were simply included in our data set. Seismic refraction and wide angle reflection profiles (Brückl et al, 2007; Šumanovac et al., 2009) had a general estimate of velocity error of ± 0.2 km/s and ± 0.1 km/s, respectively. In those cases, we simply assigned that globally estimated error to each digitized data point. In the case of the density data from the gravimetric measurements there was no error estimate. Therefore, we had to use other results in order to quantify error for that dataset. Since the only other source of density data was the NAC model, and since we had no reason to believe that the gravimetric profiles we used (Šumanovac, 2010) are of a lower quality than those included in the NAC model, we assigned the maximum error estimate (to make a conservative estimate) from the NAC model to each of the points from the digitized gravimetric profiles.

The most accurate source of velocity data were refraction and wide angle seismic reflection profiles (Brückl et al., 2007; Šumanovac et al., 2009), and the NAC model (Magrin and Rossi, 2020) but as can be seen in **Fig. 1** these studies do not cover the central and southern area of the Dinarides. Therefore, we also included velocities calculated using the values of density

from gravimetric profiles (Šumanovac, 2010). In order to calculate P-wave velocities from the available densities, we used Brocher's (2005) empirical equation:

$$V_P = 39.128\rho - 63.064\rho^2 + 37.083\rho^3 - 9.1819\rho^4 + 0.8228\rho^5,$$

355

where V_P is P-wave velocity in km/s, and ρ is density in g/cm^3. The equation is valid for densities between 2 and 3.5 g/cm^3 (with the correlation coefficient of ~0.999), the condition which was satisfied for all the densities in the gravimetric profiles used.

The velocity in the Neogene deposits is poorly known, so it was estimated using Brocher's
360 (2008) empirical relations (eqs. 1, 3, 7, and 9 in the original article). These relations account for increasing burden pressure, but not for variations in other factors. Therefore, it is justified to use these relations as a first-order approximation. We used Brocher's Plio-Quaternary relations for the shallowest parts, and relations for Paleogene–Neogene sedimentary rocks for the rest of the Neogene deposits. The values obtained ranged from 0.7
365 km/s for deposits close to surface, to 5.6 km/s at greatest depth (around 7.5 km below the surface).

We used a regional EPcrust model (Molinari and Morelli, 2011) as the underlying model in order to fill the gaps in the data coverage. The EPcrust model is represented by three layers: sedimentary cover, upper crust, and lower crust, with a horizontal resolution of 0.5° × 0.5°.
370 Each layer is characterized by laterally varying P- and S-wave velocity and density, and all of the parameters are constant for each grid point. We include EPcrust Moho, Neogene deposits bottom depth and velocity information only in parts with no other sources of data. This was done in order to remove interpolation artifacts in transition areas between the local data described before and the underlying EPcrust model. Therefore, we implemented a condition
375 to include EPcrust data in our dataset: each grid point defined in the EPcrust model had to be distanced more than 100 km in each direction from the other data point. That way, the data from the EPcrust model will not have too much influence on more relevant, local data.

For topography the SRTM15+V2.0 model (Tozer et al., 2019) was used. It is an updated global elevation grid at a spatial sampling of 15 arc seconds, and it also includes bathymetry.
380 Since the grid of the SRTM15+V2.0 model is much more refined than the grid we used for the definition of the model (15 arc seconds in the topography model compared to about 3 arc minutes in our model), a regridding has been performed by averaging all the values that fall inside one model cell.

After collecting and preparing the data, the next step was interpolation. Ordinary kriging was
385 used to interpolate model interfaces and universal kriging when interpolating the layer properties (Vp velocity, density), as the layer properties are linearly dependent on depth (for details please see Appendix C). After interpolation, we filtered Moho interface and layer properties with a 100-km wide Gaussian filter to smooth the transitions between different

data sources. The smoothing in case of the Neogene deposits and CRC interfaces was omitted because the data used came from similar sources, and smoothing would conceal structures with relatively small spatial dimensions (e.g. Sava and Drava depressions).

Finally, we observed how the smoothing influences crustal velocity, particularly in the area covered only by gravimetric profiles. Given that the gravimetric profiles are interpreted in terms of homogeneous sections and given that the smaller sections interpreted were roughly about 100 km in dimension along the profile, we chose this as the Gaussian width. It was also confirmed by trial and error that below this width we would observe some artifacts in the model. Model uncertainty was estimated as the sum of two components: uncertainty in the input data and uncertainty from the interpolation.

Results

Since the model is mostly concentrated on the Dinarides where the topmost cover is predominantly made of Paleozoic–Eocene CRC, Neogene sedimentary cover is negligible for the large part of the model, but areas to the east and northeast of the Dinarides (i.e. SW Pannonian Basin) have thick Neogene deposits reaching thicknesses of more than 4 km. Here, the most prominent features, clearly seen as two red bands in **Fig. 3a,** are the Sava and Drava depressions, with Drava depression being slightly deeper.

CRC bottom depth model (**Fig. 3c**) is almost a reverse image of the Neogene deposits bottom model. In the SW Pannonian Basin, where Neogene deposits are the thickest, the underlying carbonate layer is thin, and vice versa – in the Dinarides, where the CRC is the thickest, there are no prominent Neogene deposits. CRC thickness is well over 5 km in the northern part of the External Dinarides and thickening southwards reaching cumulative thicknesses of almost 15 km in the southern Dinarides. In the Adriatic Sea area, carbonates are thinning out towards southwest, but this may be partly caused by lack of available data in that part of the model.

The greatest Moho depths in the investigated region are found in the SE part of the Dinarides, reaching depths of over 45 km (see **Fig. 3e**). To the NW, along the External Dinarides, the Moho becomes shallower, reaching depths of around 40 km. In the SW part of the Pannonian basin, the crustal thickness is between 20 and 30 km, becoming even shallower going further east. In the Adriatic Sea (within the part covered with our model), the Moho is shallower than in the Dinarides, but deeper than in the SW Pannonian Basin, with crustal thicknesses between 30 and 35 km. At the transition between the Adriatic Sea and the Dinarides, the Moho depth change is gradual, whereas going towards the SW Pannonian basin from the Dinarides, the change is rather abrupt.

Given that a significant contribution to the uncertainty value is from the interpolation itself (which is of greater value at grid points further away from the input data points), one can distinctly see the areas with less data coverage as areas with higher uncertainty. Moho depth uncertainty (**Fig. 3f**) is low in the entire area of interest, i.e. the wider Dinarides region. For Neogene deposits bottom the area of lower data coverage is in the eastern part of the Internal Dinarides where there is less information available on sedimentary thickness (**Fig. 3b** but see also **Fig. 1**). On the other hand, that part of the Internal Dinarides is mostly covered by the exposed bedrock largely composed of low-grade metamorphic Paleozoic–Mesozoic formations with thin cover of Mesozoic CRC (e.g. Schmid et al., 2008), so Neogene deposits thickness values here are mostly negligible. For the CRC thickness, the area of least accuracy is in the NE part of the investigated area (junction zone between Dinarides-Pannonian basin - Southern Alps). Similar to the previous case, here the low accuracy is due to the lack of measurements on CRC thickness as the region is covered by a thick layer of Neogene deposits.
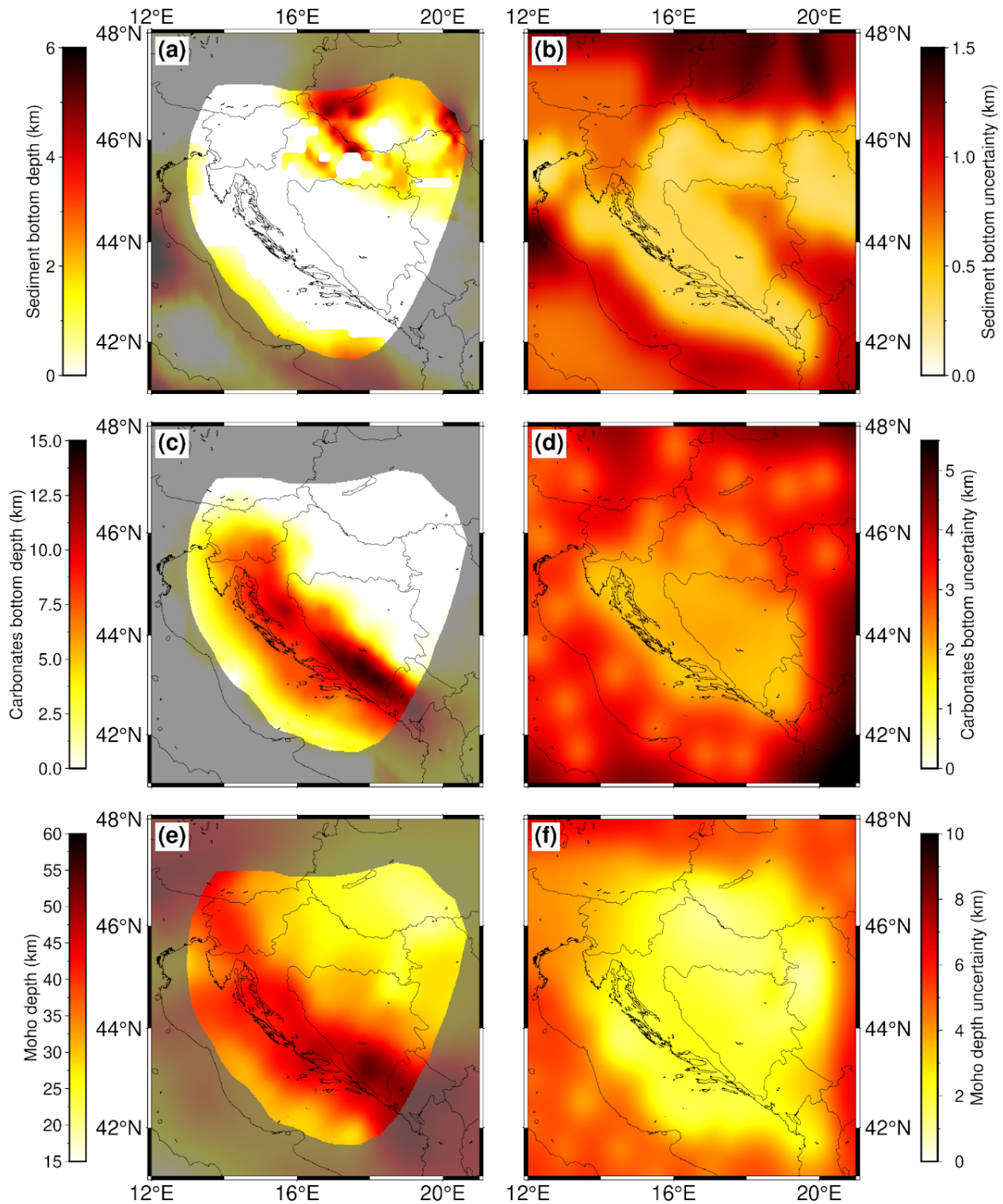
**Figure 3.** Model interface depths and corresponding uncertainties: (a) Neogene deposits bottom depth, (b) Neogene deposits bottom uncertainty, (c) CRC bottom depth, (d) CRC bottom uncertainty, (e) Moho discontinuity depth, and (f) Moho depth uncertainty. Depths are defined as kilometers below sea level and the areas of lower resolution are shaded.

440

445　The seismic velocity distribution within the model is depicted in the left-hand side of **Fig. 4** at four depths (5, 10, 20 and 30 km) showing most prominent features of the model crustal structure. At a depth of 5 km (**Fig. 4a**), the P-wave velocity in a large part of the External Dinarides is about 6 km/s. Given that we had no independent estimate for the velocity for the CRC, we cannot discern it as a separate layer just looking at velocity values. Outside the

450　External Dinarides, one can see that the velocity in the SW Pannonian Basin at depth of 5 km is slightly lower (just below 6 km/s) than than in the rest of the investigated area.

At a depth of 10 km (**Fig. 4c**) the velocity values in the SW Pannonian Basin are considerably lower than in the rest of the model, with values around 6 km/s. In the area of the Internal Dinarides, velocity at 10 km depth is slightly higher than in the External Dinarides and

455　beneath the Adriatic Sea. It is hard to discern if this reflects the actual structure, or if it is the consequence of the higher uncertainty in that part of the model (the velocity here was estimated from the density values from the gravimetric profiles, given that there were no other data sources available). Similar situation can be seen in **Fig. 4e** for a depth of 20 km. For this depth the velocities in the SW Pannonian Basin are reaching values above 6 km/s

460　whereas values for the Dinarides are again higher (especially in the internal part) than in the rest of the investigated area, with values above 6.5 km/s. In the lower part of the crust (**Fig. 4g**) at a depth of 30 km in the central part of the Dinarides the P-velocity values are reaching 7 km/s.

In the same image the mantle velocity values are shown in grayscale due to the considerable

465　difference between crust and mantle values and the fact that the crustal thickness in SW Pannonian basin is mostly less than 25 km. The mantle velocity variations are better seen in profile sections (e.g. **Fig. 5f**). At the 30 km depth level, the velocity is much higher in the southern External Dinarides and below the Adriatic Sea (at least the part covered with our model) than in the northern External Dinarides.

470　**Fig. 4** also shows error estimates for P-wave velocity. It can be seen that the lowest estimates are in the area where we used the NAC model input data (Magrin and Rossi, 2020), and in areas where data from active seismic profiles were available (Brückl et al., 2007; Šumanovac et al., 2009). The distribution of the errors shown in **Fig. 4** was expected given the fact that the digital NAC model and the active seismic profiles are of highest quality and that

475　gravimetric data has higher uncertainty. Estimated uncertainty is highest in the area where gravimetric profiles (Šumanovac, 2010) are the main source of the data used to infer P-velocity.
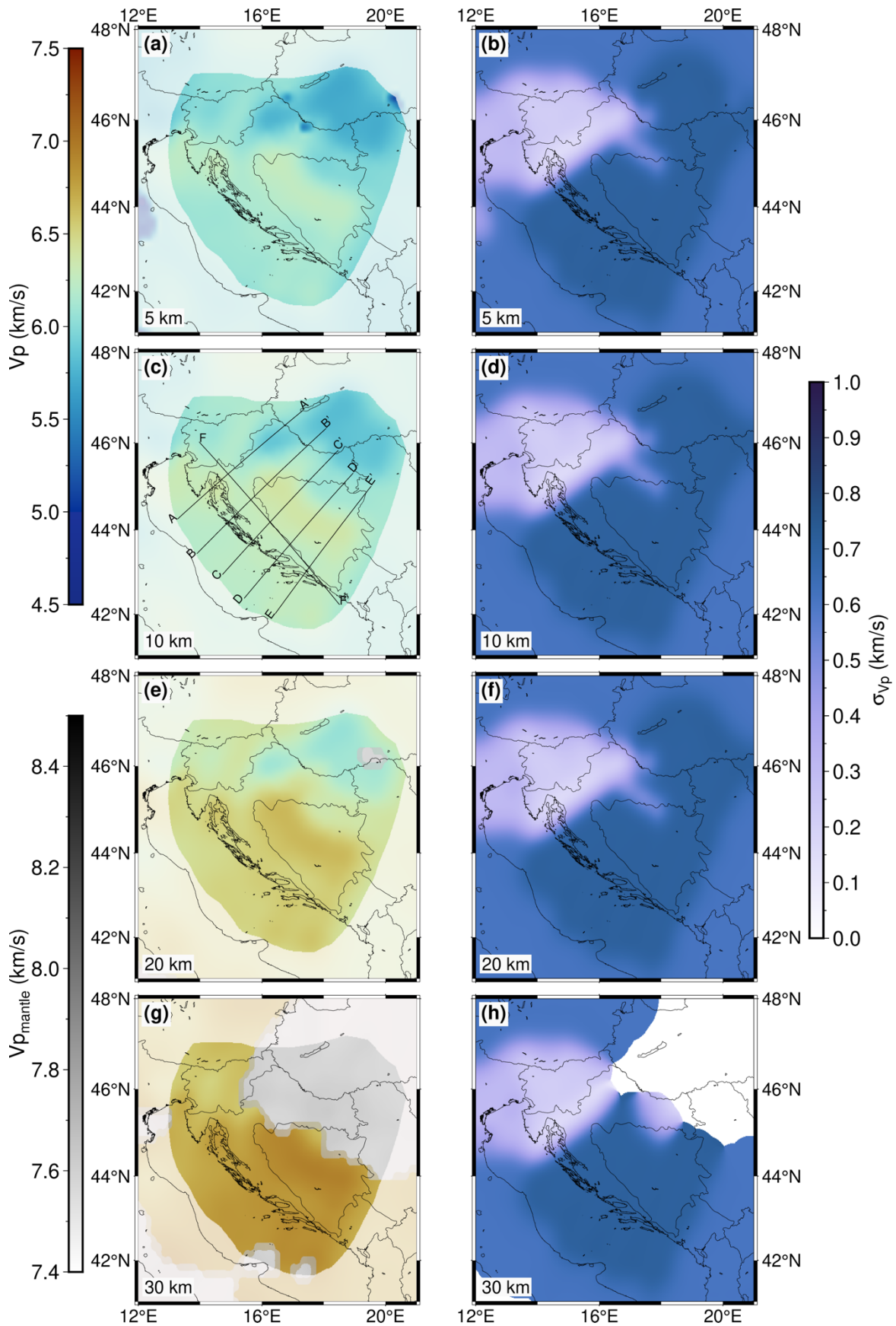
Figure 4. Velocity model depth slices and corresponding uncertainties for 5 km, 10 km, 20 km, and 30 km depth (below sea level) are shown in panels (a)(b), (c)(d), (e)(f) and (g)(h). In the panel (c) the positions of the profiles shown in **Fig. 5** are marked**. The areas of lower resolution are shaded, and the gray color scale corresponds to the mantle velocity (see text for details).

Fig. 5 shows depth variations of velocity along five profiles crossing the Dinarides perpendicularly and one profile (FF)' running parallel to the main strike of the mountain chain (locations marked in **Fig. 4c**). Profile AA' (**Fig. 5a**) crosses the Dinarides in their northern part. The maximum Moho depth below the Dinarides on this profile (around 40 km) is the lowest compared to the other profiles. At a distance of ~270 km, the profile reaches the SW Pannonian Basin, which can be clearly seen by a thinning of the crust (between 20 and 30 km) and by the topmost layer of Neogene deposits of lower P-velocity. Although the CRC thickness is indicated with the dashed line, one cannot recognize the transition into this unit by looking just at the velocity values. Generally, the velocities in the part of the profile crossing the Dinarides are larger than in the part of the profile crossing the SW Pannonian Basin. The velocity gradually increases with depth, reaching values of about 6.7–7.0 km/s in the deepest part of the crust, with the exception of the SW Pannonian Basin, where the velocity just above Moho is lower, about 6.5 km/s.

The maximum Moho depth seen on profile BB' (**Fig. 5b**) is somewhat greater than in profile AA', a little over 40 km in the part of the External Dinarides. It is shallower in the Adriatic area (in the first 50 km of the profile) and in the Internal Dinarides (after about 220 km). At the very end of the profile, where it reaches the SW Pannonian Basin, one can see a similar feature as seen in profile AA': thinner crust and slightly lower velocity just above Moho than in the rest of the profile. In the same profile the largest CRC thickness, indicated by the dashed line, coincides with the deepest Moho and closely follows the velocity isoline of about 6.3 km/s. That feature can also be observed on other profiles (CC' and DD') at similar locations.

The profile CC' (**Fig. 5c**) crosses the Dinarides in their central part. Here the maximum Moho depth is almost 50 km. The profile reaches the SW Pannonian Basin only in the last 100 km, but it covers much of the Internal Dinarides. The CRC is of uniform thickness along the part of the profile covering the Dinarides (the first 100 km cover the Adriatic Sea area). The crust is thickest beneath the External Dinarides, and is becoming thinner going both towards the Adriatic Sea and the Internal Dinarides. In this central part of the External Dinarides, there is also relatively higher velocity deeper in the crust, 7.0–7.2 km/s, just above the Moho. In the Internal Dinarides (between 250 to 300 km from the start of the profile), the velocity just above the Moho is a little lower than in the external part, around 6.7–7.0 km/s. As noticed in the previous two profiles, the velocity just above Moho in the SW Pannonian Basin is even lower than in the Internal Dinarides. Similar to the profile BB', the bottom of the CRC

19

coincides with the velocity values of about 6.2–6.3 km/s, except in the very beginning of the profile (first ~50 km).

Profiles DD' and EE' (**Fig. 5d and 5e**) cross the southernmost part of the Dinarides. Here, the Moho reaches depths of >50 km. Also, the crustal velocity at those depths is larger compared to all the other profiles, reaching almost 7.5 km/s. Variations in Moho depths and crustal velocity along the mountain chain can be best seen in the profile FF' (**Fig. 5f**), running parallel to the Dinarides from northwest to southeast. In this profile, Moho depth increases from around 40 km in the northern part to >50 km in the southern part. Also, the crustal velocity just above Moho changes from just below 7.0 km/s in the north to almost 7.5 km/s in the south. Similarly, velocity in the mid-crustal zone (~20–25 km depth) is somewhat lower in the northern part of the profile, a little over 6.5 km/s, but becomes higher in the southeastern part reaching values of about 7 km/s.
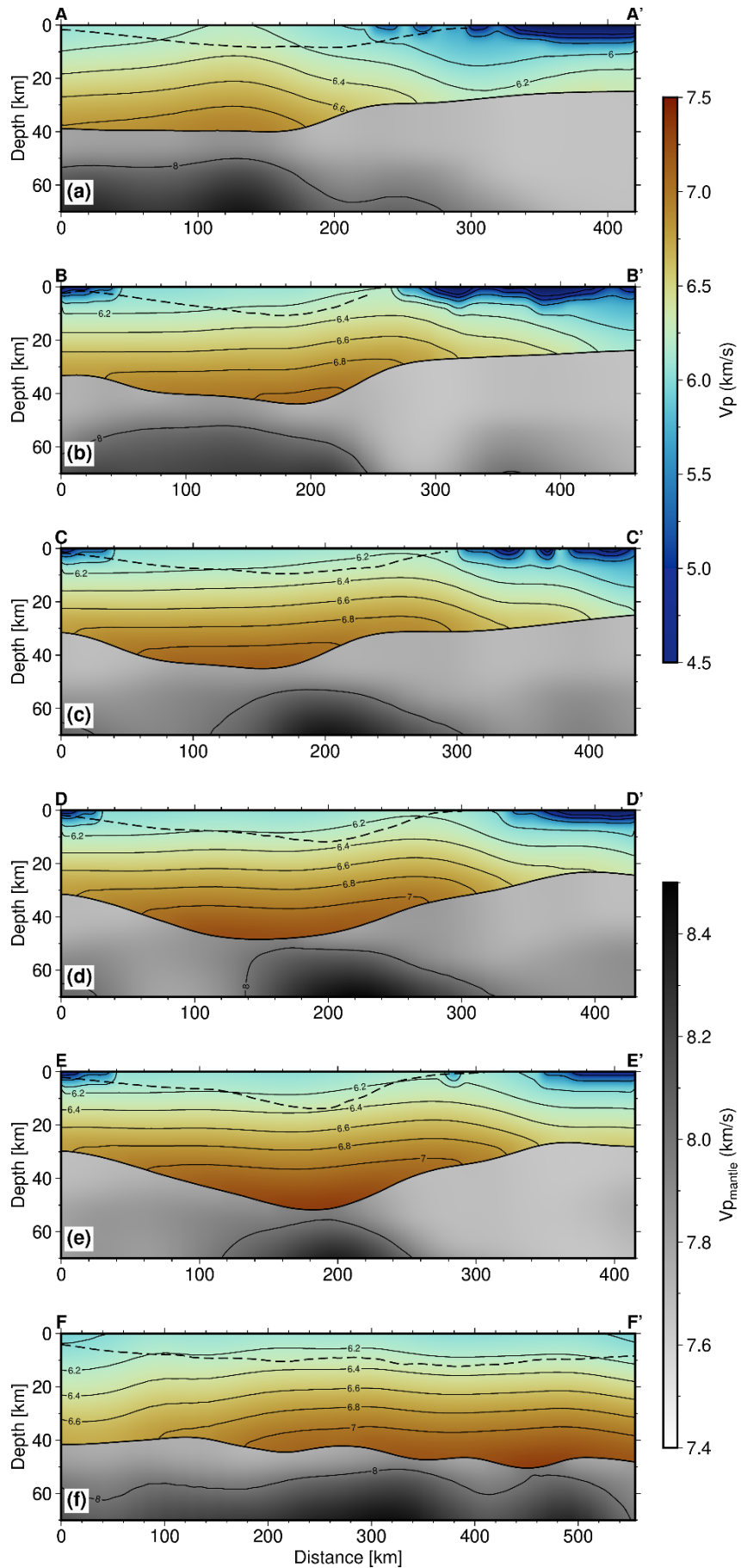
Figure 5. Profiles with locations shown in **Fig. 4c**: (a) AA'; (b) BB'; (c) CC'; (d) DD'; (e) EE', and (f) FF'. Parallel full lines running along the profile are the velocity isolines. The depth of the CRC as derived from known geological data is indicated as the dashed line close to the surface.

535 From the NAC model (Magrin and Rossi, 2020) and the gravimetric profiles (Šumanovac, 2010), we have interpolated the density values for the entire crust (**Fig. 6**). Keep in mind that for this interpolation there were only two sources of data, one of which had densities defined as layers homogenous in density (Šumanovac, 2010). Therefore, this parameter is much less accurate than P-wave velocity. It can be seen that the density is slightly higher in the area of 540 the Internal Dinarides than in the External Dinarides for all the depths considered here, possibly coinciding with higher density crystalline crust. In the SW Pannonian Basin, the density has much lower values.
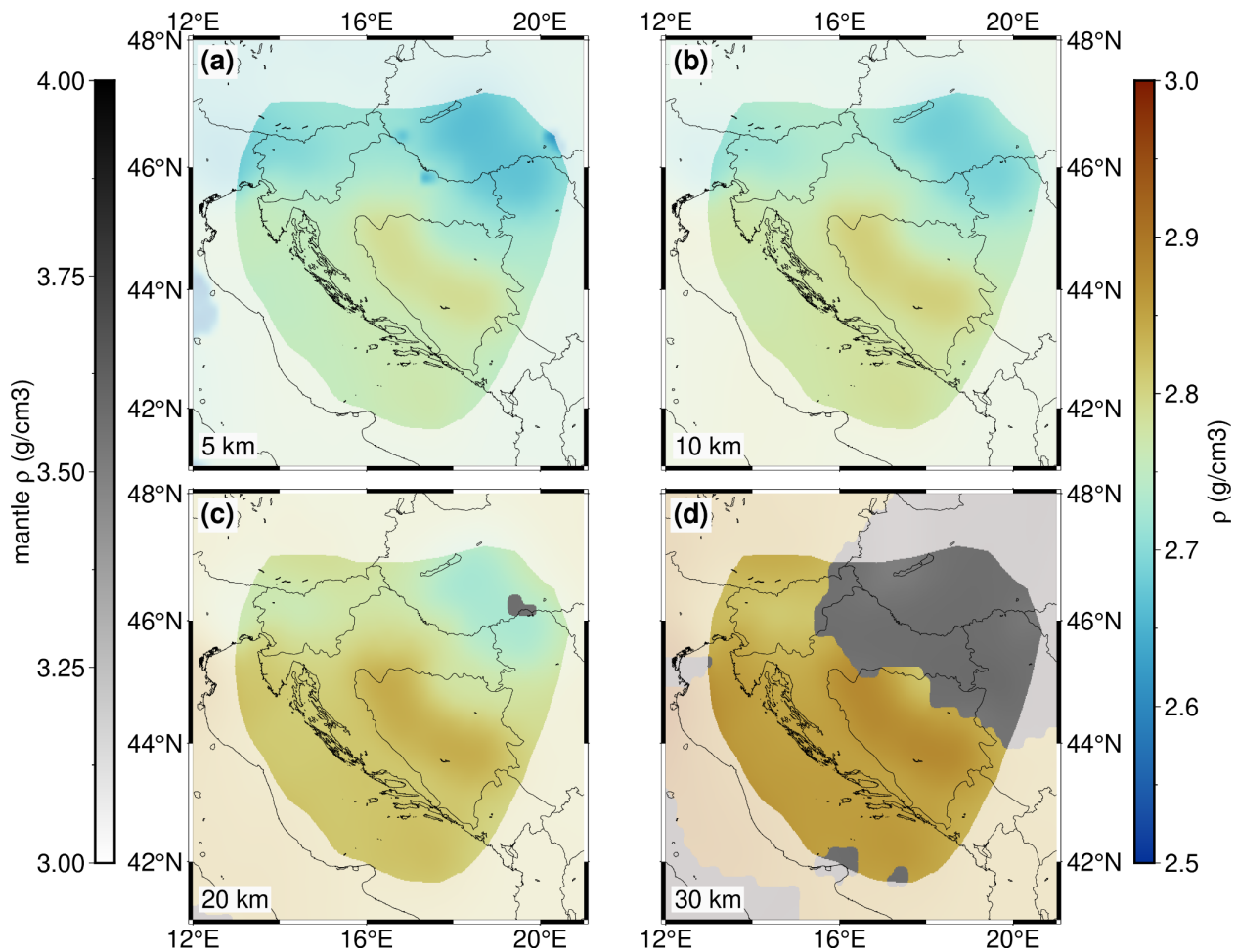
545 **Figure 6.** Density model depth slices for (a) 5 km, (b) 10 km, (c) 20 km, and (d) 30 km depth. The areas of lower resolution are shaded, and the gray color scale corresponds to the mantle density (see text for details)

22

In the case of S-wave velocity, there was no measured velocity data (the only available Vs results were from the NAC model which covers the western corner of our study area) so these values were estimated using the P-wave velocity and another set of Brocher's (2005) empirical relation connecting P- and S-wave velocity (**Fig. 7**).
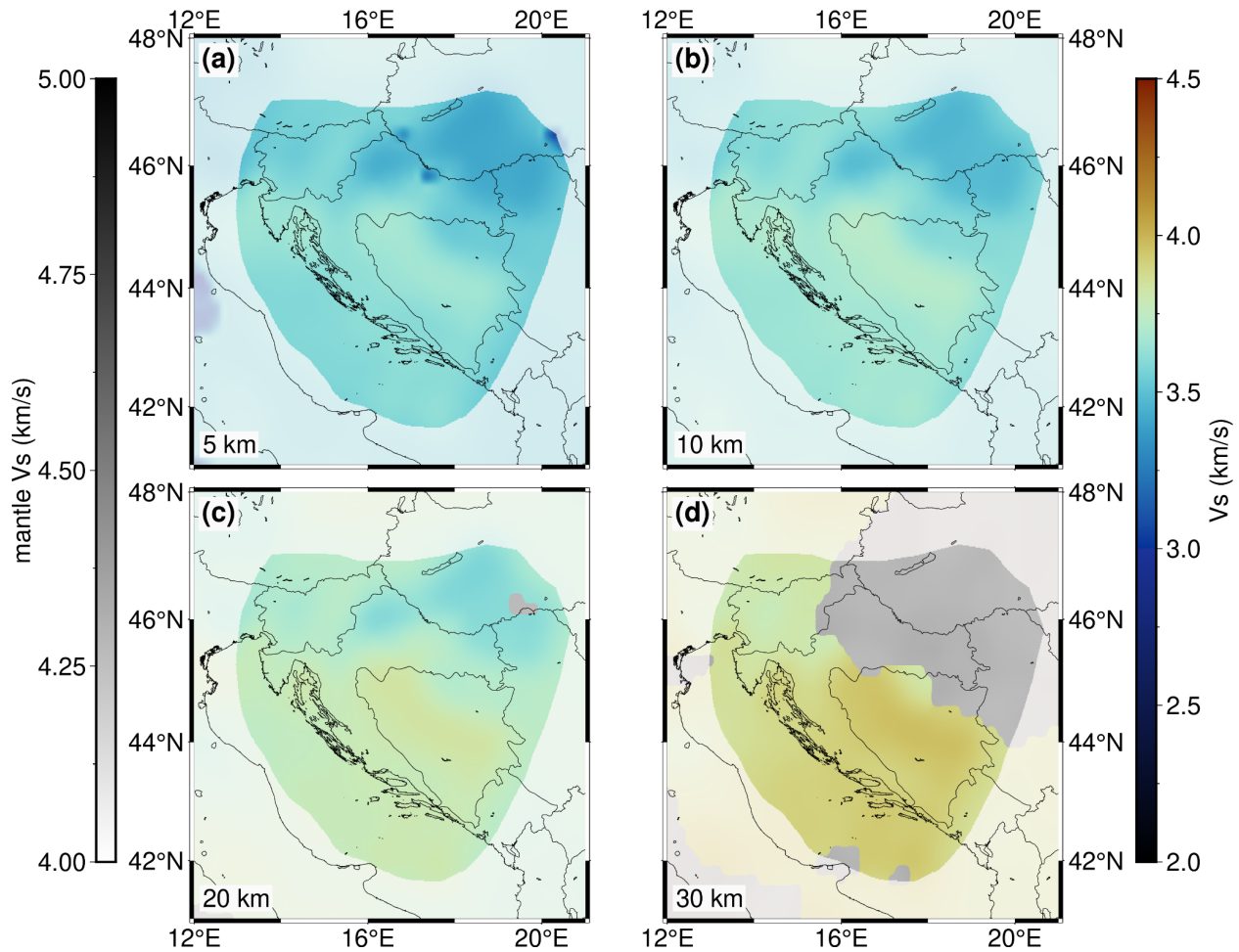
Figure 7. S-wave velocity depth slices for (a) 5 km, (b) 10 km, (c) 20 km, and (d) 30 km depth. The areas of lower resolution are shaded, and the gray color scale corresponds to the mantle velocity (see text for details).

Model testing

To test how well the newly derived 3-D model represents the true structure, we calculated the travel times for a regional earthquake recorded on representative seismic stations in the wider Dinarides area (**Fig. 8**). We also calculated travel times using the simple 1D model with two isotropic crust layers currently employed for routine earthquake locating in Croatia (B.C.I.S. (1972), Herak et al., 1996). The 1D model's topmost layer is characterized by P-velocity of 5.8 km/s, and the deeper crustal layer has the P-wave velocity of 6.65 km/s. For the same model the uppermost mantle velocity is 8.0 km/s. We then compared the travel times from both models with the true measured travel times. We used the Pn and Pg phases of the 2020 Petrinja M_w6.4 earthquake. The location of the earthquake (42.4188 °N, 16.2082 °E, 7.57 km) and the stations that recorded the wave onsets are shown in **Fig. 8**. For travel time calculation we used the Fast Marching Method (de Kool et al., 2006) as implemented within the FMTOMO package (Rawlinson and Urvoy, 2006).
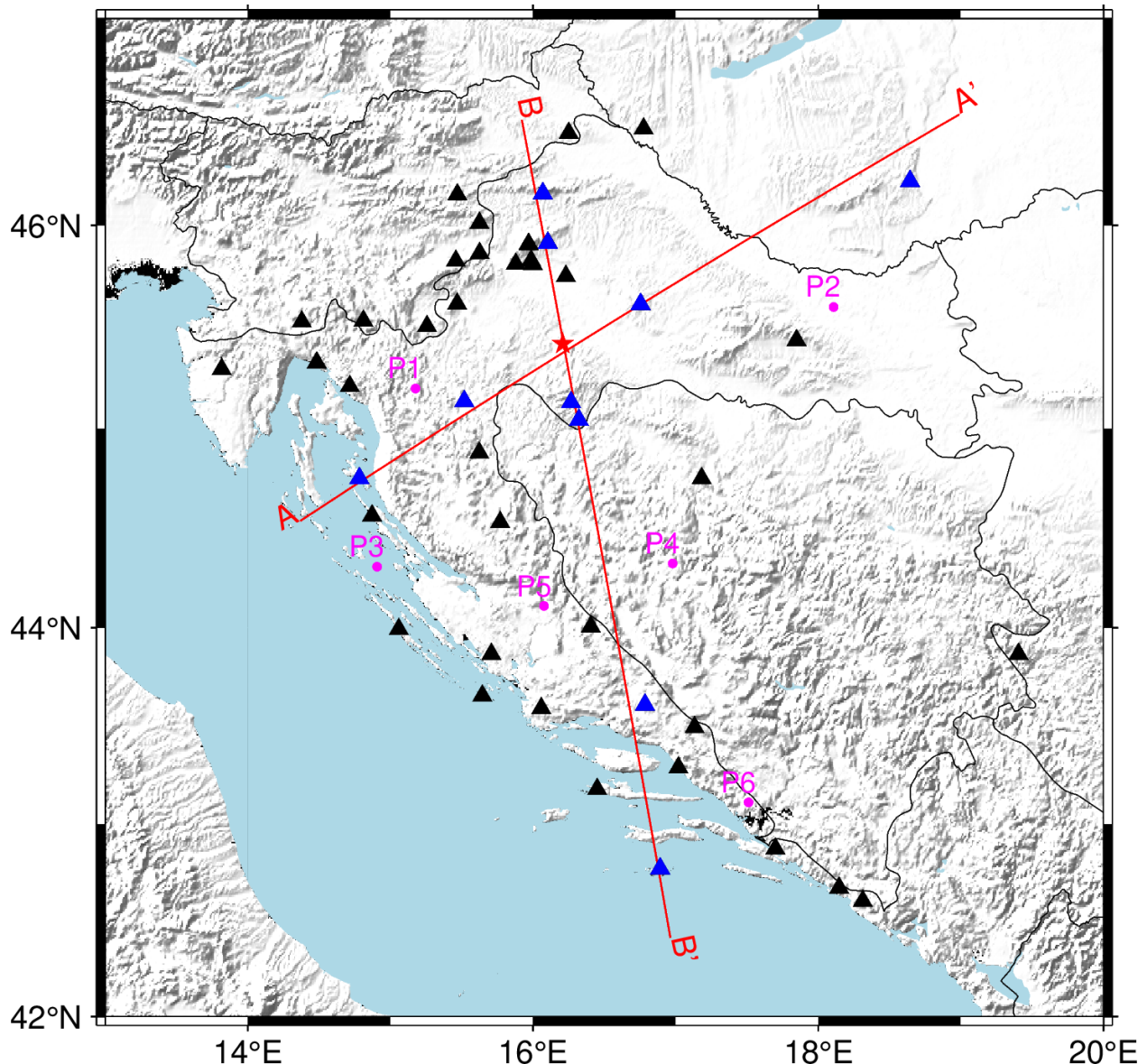
Figure 8. Epicenter of the Petrinja 2020 earthquake sequence mainshock (red star) and stations used for calculation of traveltimes (black and blue triangles). Travel times for all the stations are shown in **Figs. 9** and **10**. The red lines mark the positions of the cross sections shown in **Fig. 11** (section AA') and **Fig. 12** (section BB'). The stations coloured blue are the ones shown in **Fig. 11** and **Fig. 12**. The points colored in magenta mark the position of 1D models shown in **Fig. 13**.

Figures 9 and 10 show the differences in travel times calculated between the models (both 1D and 3-D) and observed travel times for Pg and Pn phases, respectively. When looking at Pg phases (**Fig. 9**), we can see improvement in calculated travel time accuracy when using the 3-D model (with respect to the 1-D model) for epicentral distances smaller than 50 km and over 100 km. For smaller epicentral distances, the more accurate travel times in the 3-D model are connected with better specification of Neogene sedimentary cover with low P-wave velocity. On the other hand, for epicentral distances between 50 and 80 km 1D and 3-

25

D models travel times are similarly offset compared to the observed travel times, with times calculated using the 1D model being slightly more accurate. We believe this is due to the less accurate velocity sampling in the upper crust in the transitional zone between Internal Dinarides and SW Pannonian Basin and lack of knowledge about spatial coverage of the CRC in this area. For greater epicentral distances we can see that travel times calculated using the 3-D model are much more accurate compared to those calculated using the 1D model. That means that the crustal velocity derived in our 3-D model is a considerable improvement of the simple 1D model.
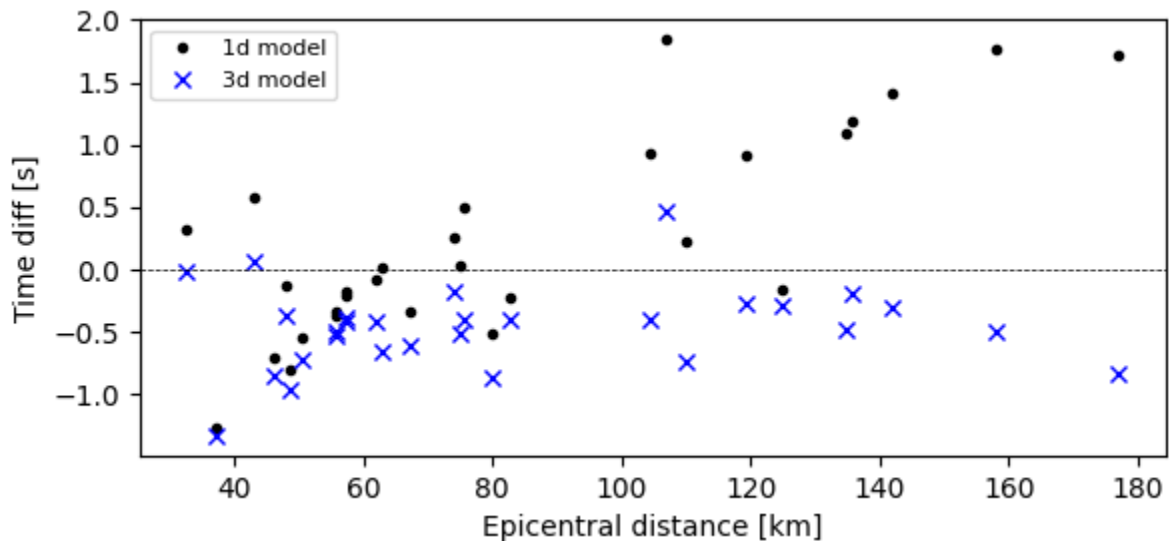
Figure 9. Pg phase travel times for the 2020 Petrinja earthquake: time difference between 1D model and observed travel times (black dots) and between 3-D model and observed travel times (blue crosses).

Concerning the Pn phases (**Fig. 10**), we can see that the travel times calculated using the 3-D model are generally closer to the actual observed travel times for all the epicentral distances shown than those calculated using the 1D model. In case of Pn phases, the uppermost mantle velocity plays a great part in the total travel times, so both the crustal model we derived here and the mantle model from Belinić et al. (2020) show improvement compared to the 1D model. There is still room for improvement in the uppermost mantle velocity since the model of Belinić et al. (2020) we used here is most accurate for greater depths (80–100 km).
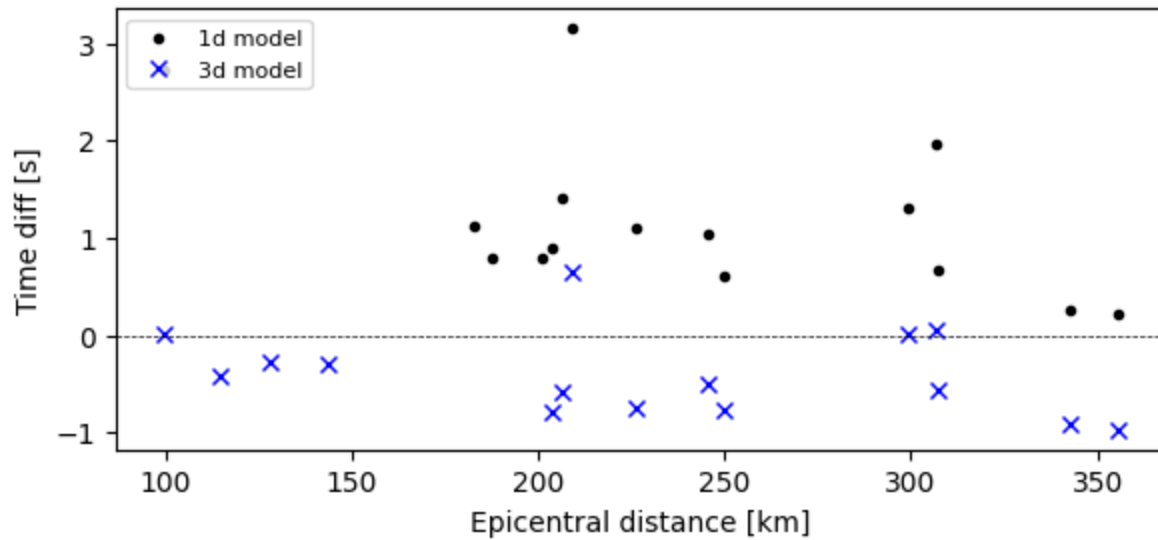
Figure 10. Pn phase travel times for the 2020 Petrinja earthquake: time difference between 1D model and observed travel times (black dots) and between 3-D model and observed travel times (blue crosses).

Figure 11 shows a cross section AA' (location in **Fig. 8**) of the newly derived 3-D model, with the calculated ray paths using the simple 1D and 3-D models. The position of the section was chosen in order to show travel times for both Pg and Pn phases, and we also tried to position it in such a way that it crosses almost perpendicularly the main strike of the Dinarides. There is also another cross section shown in **Fig. 12** (BB'), oriented approximately north to south. Positions of the stations shown in cross section BB' are also marked in **Fig. 8**. From both profiles it can be seen that the seismic rays cover completely different paths depending on whether they were calculated using the 1D or the 3-D model. For example, the Pg phases, when calculated using the 3-D model, travel much deeper than their 1D counterparts. Also, since the Moho in the Pannonian Basin of our 3-D model is much shallower than the Moho in the simple 1D model, the calculated rays using either 1D or 3-D model travel on very different paths in the uppermost mantle. That is particularly visible in **Fig. 12**, in case of the ray path between the source and the most distant station shown. The ray path calculated for the 3-D model reaches depths of almost 60 km, while the same ray path calculated for the 1D model reaches depths of only 40 km. Given all that, it can be concluded that precise knowledge about the crustal model is very important for all seismic applications.
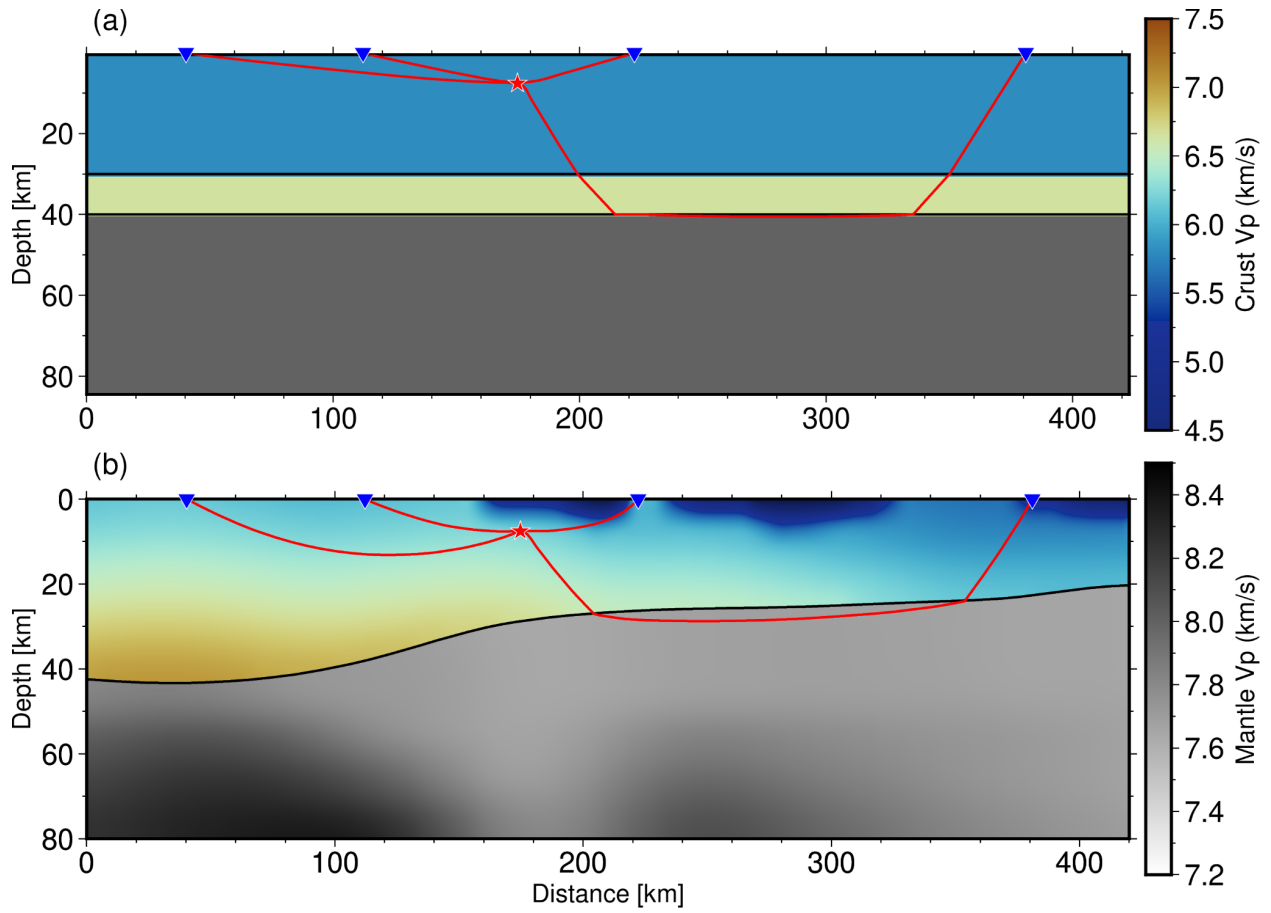
Figure 11. Earthquake ray paths in cross section AA' (for location see **Fig. 8**) for two models: (a) a simple 1D model with two isotropic crustal layers, and (b) our 3-D model with one anisotropic crustal layer. Colorbars are the same for both panels.

630

Figure 12. Earthquake ray paths in cross section BB' (for location see **Fig. 8**) for two models: (a) a simple 1D model with two isotropic crustal layers, and (b) our 3-D model with one anisotropic crustal layer. Colorbars are the same for both panels.
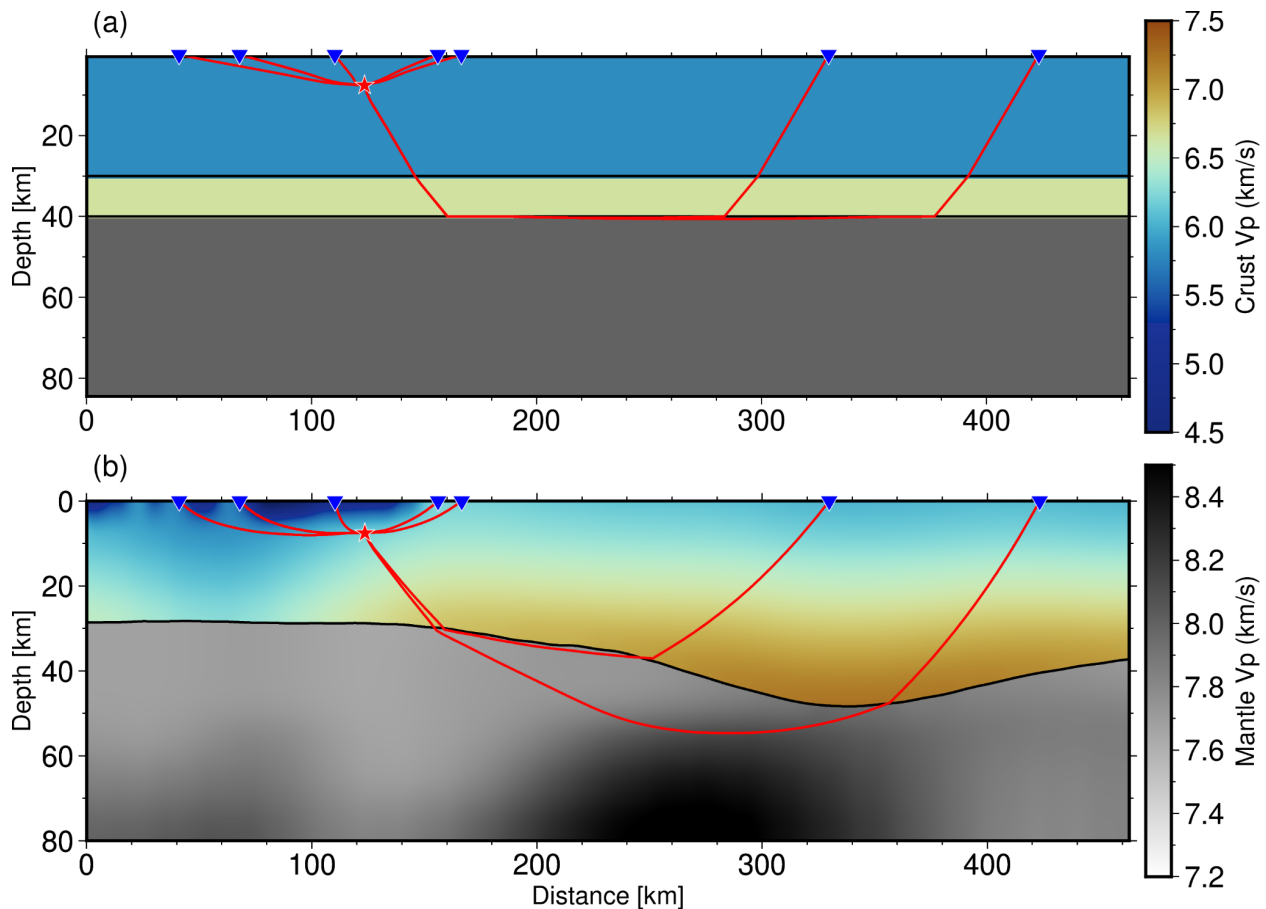
635

In addition to the profiles shown in **Figs. 11** and **12**, we also extracted depth velocity curves from the new 3-D model for six points marked in **Fig. 8** in magenta. Those six points have been chosen to cover different domains of our model (Stable Adria, Internal and External Dinarides, and the SW Pannonian Basin). For example, at the P2 point (**see Fig. 13b**), which is located in the SW Pannonian Basin, the velocity in the first couple of kilometers is much lower than for the other points because there is a Neogene deposits layer on top. The course of the curve of each model shown in **Fig. 13** is generally similar at each point with obvious differences being Moho depth (see points P2 and P1) and rate of increase of velocity with depth (e.g., compare points P3 and P5).

640

29
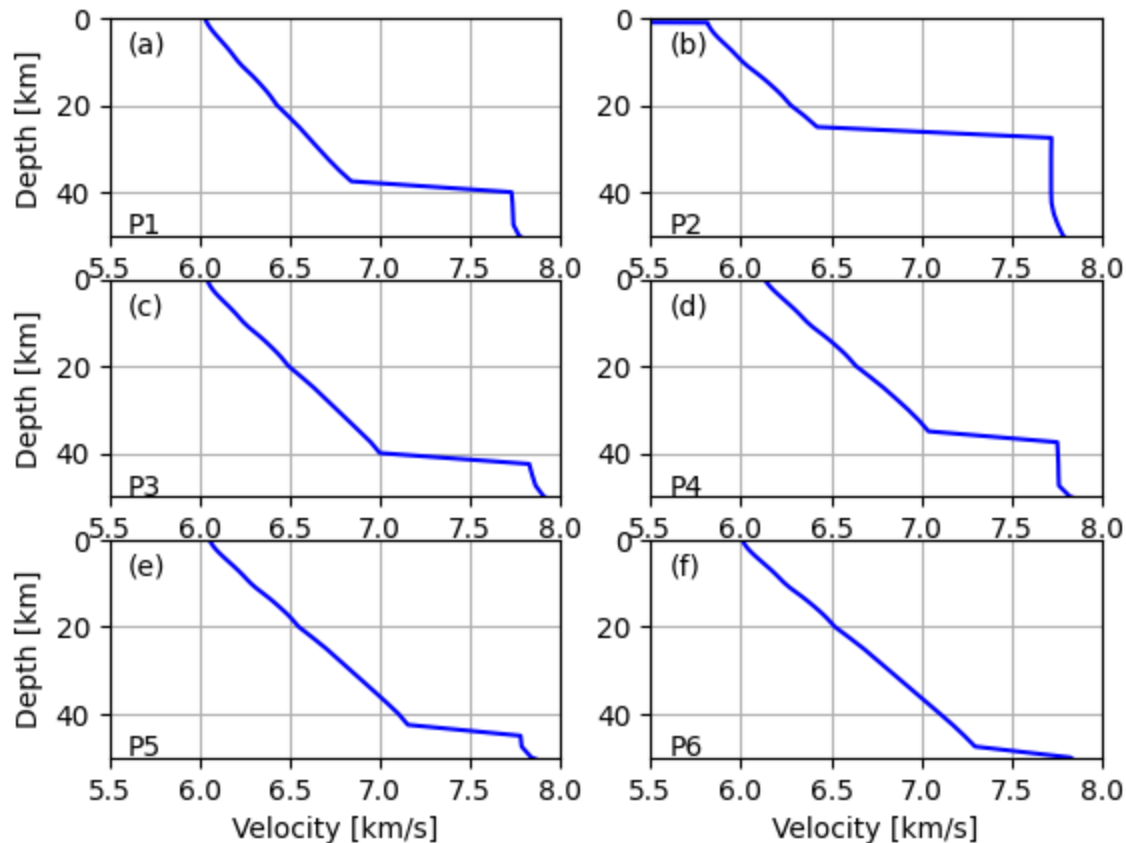
Figure 13. Velocity changes with depth for six points (P1 to P6; for locations see **Fig. 8**).

Discussion

The creation of the presented model was motivated by the need for a more complete 3-D seismic model of the Dinarides. Although there have been previous studies estimating various properties of the crust in the region, a seismic model of the Dinarides crust and upper mantle did not exist until this study. In this work we assembled data from previous investigations to create a first comprehensive model of the crust for the wider Dinarides area. The Moho depth is the best constrained parameter of this model, since there were several good sources of high-quality data regarding this parameter. It confirms what we already know about the Moho in the Dinarides, but now it is presented as a comprehensive, ready-to-use model.

For the Neogene deposit thickness, we used manually digitized maps, therefore having less precise data, but which were originally created from a high number of active seismic profiles and thus strengthening our confidence that this parameter was adequately presented in our

30

model. The thickest Neogene sedimentary cover can be found in the area of the Sava and Drava depressions with thinner cover in the rest of the SW Pannonian basin and almost non-existent in other regions, most notably in the Dinarides, as well as in some hilly areas of the SW Pannonian Basin.

665　As can be seen in **Fig. 1**, all the P-wave velocity high-quality data are concentrated in the NW part of the study area. In the southern part, we relied on the inverted gravimetric profile data (Šumanovac, 2010), which is not the ideal data source due to the high uncertainties and lower resolution. Nevertheless, given the lack of other data sources for South Dinarides, even the data from the gravimetric profiles proved to be of high value. It seems that the velocity

670　in the Internal Dinarides, where we only had inverted gravimetric profile data available, is slightly higher than in the rest of the model. At this point, we cannot discern if it is an actual feature, or some artifact due to lower quality data. The fact is that this is a separate structural unit originating from different tectonic processes, so it is not impossible that it has different features and lithological properties. If these data were omitted from the interpolation, we

675　would have even worse results, because in that case the values would be purely extrapolated. The approach we chose gave at least some constraint to the velocity values in this part of the model.

It is interesting to note that the trend of velocity in the lower part of the crust corresponds to the velocity trends in the uppermost mantle. There is a positive velocity anomaly in the

680　part of the uppermost mantle right below (or slightly offset from) the part of the crust with the deepest Moho. These positive anomalies in the work of Belinić et al. (2020) have been interpreted as a signal of the subducting Adria Microplate. Our model is mere interpolation of what was already known, but perhaps what we see here is part of the Adria crust being dragged along with the uppermost part of the mantle in the subduction below the Dinarides.

685　As can be seen in the profile shown in **Fig. 5a**, in the SW Pannonian basin, the crustal velocity is much lower than in the Dinarides, a feature also observed by Šumanovac et al. (2009). Perhaps the lower velocity is a feature of the Pannonian crust, whereas the relatively higher crustal velocity is a feature of the Adria crust. To make a definitive conclusion, more investigation should be performed.

690　The velocity estimation for the Neogene deposits and the Mesozoic carbonates proved particularly challenging since there is little available data about this parameter. In the case of Neogene deposits, we used Brocher's (2008) relation for the deposits of similar age. For the CRC we could not derive any velocity–depth relation due to the lack of available data, so in this case, we simply used the same velocity interpolation as for the rest of the crust. It

695　seems, though, that at least in some parts of our new model, the CRC bottom depth coincides with the velocity of around 6.2 - 6.3 km/s.

Conclusions

Having a 3-D model of the crustal structure is a major step forward in the study of the Dinarides and the surrounding areas. The newly derived model is defined on a regular grid for three key parameters (P- and S-velocity and density), and as such can be readily used by seismologists who need information on crustal structure as input for their studies (earthquake locating, seismic tomography, shaking estimation, seismic hazard…). We tested the performance of the model in comparison with the commonly used 1D model and found significant improvements in time travel calculations. The model still has some inherent weaknesses that have been discussed in the previous sections which are mostly connected with the limited existence of measurements in some parts of the region. Nevertheless, the 3-D model represents a good first step towards improving the knowledge of the crustal structure in the complex area of the Dinarides.

The model clearly delimits several key areas (Dinarides, Pannonian Basin and Adriatic Sea) as well as distinguishes distinct layers in those regions (i.e., Neogene deposits and CRC). The most robust feature of the model is the depth to Mohorovičić discontinuity, but other parameters are also reasonably well defined. Inclusion of the CRC thickness is, to the best of our knowledge, the first attempt to estimate this parameter for the whole Dinarides region. One of the new insights found during the creation of the model is the relatively high (P-wave) velocity for the lower crust in the southern part of the Dinarides. This feature needs to be confirmed by other studies, given the sparsity of information about velocity for that region. On the other hand, the high velocity feature fits nicely to the higher velocity of the uppermost mantle found in the same area, thus corroborating the idea of continental subduction (and/or lithospheric delamination) in south-central External Dinarides.

In conclusion, the model presented here represents the currently best and most complete crustal model for the wider Dinarides region. The model is assembled from all the available measurements on seismic velocity, density, layer composition and thickness to provide a full representation of the major variations of seismic wavespeeds in the regional crust. Hopefully, the new 3-D model will help discover some new, previously unknown features of the crust and in turn, each new study that sheds some light on the crustal structure in this area may improve the 3-D model derived here.

Resources

The model derived in this work is available on the following link: https://urn.nsk.hr/urn:nbn:hr:217:793485

Acknowledgements

References

Aljinović, B.: Najdublji seizmički horizonti sjeveroistočnog Jadrana, Ph. D. thesis (in Croatian with English abstract), University of Zagreb, Croatia, 219 pp., 1983.

Aljinović, B., Prelogović, E., and Skoko, D.: New data on deep geological structure and seismotectonic active zones in region of Yugoslavia, Boll. di Oceanol. Teorica ed Applicata, 2, 77–90, 1987.

Annoni A., Luzet C., Gubler E, and Ihde J.: Map Projections for Europe, European Commission Joint Research Centre, reference EUR 20120 EN, 2003.

Artemieva, Irina M., and Thybo, H.: EUNAseis: A seismic model for Moho and crustal structure in Europe, Greenland and the North Atlantic region, Tectonophysics, 609, 97–105, http://dx.doi.org/10.1016/j.tecto.2013.08.004, 2013.

Balling, P., Tomljenović, B., Schmid, S. M., and Ustaszewski, K.: Contrasting along-strike deformation styles in the central external Dinarides assessed by balanced cross-sections: implications for the tectonic evolution of its Paleogene flexural foreland basin system, *Global Planetary Change*, 205, 103587, https://doi.org/10.1016/j.gloplacha.2021.103587, 2021.

B. C. I. S. (1972): Tables des temps des ondes séismiques. Hodochrones pour la region des Balkans (Manuel d'utilisation). Strasbourg.

Belinić, T., Stipčević, J., Živčić, M., and the AlpArrayWorking Group: Lithospheric thickness under the Dinarides, Earth and Planetary Science Letters, 484, 229–240, https://doi.org/10.1016/j.epsl.2017.12.030, 2018.

Belinić, T., Kolínský, P., Stipčević, J., and AlpArray Working Group: Shear-wave velocity structure beneath the Dinarides from the inversion of Rayleigh-wave dispersion, Earth and Planetary Sciences Letters, 555, https://doi.org/10.1016/j.epsl.2020.116686, 2020.

Brocher, T. M.: Empirical relations between elastic wavespeeds and density in the Earth's crust, Bulletin of the Seismological Society of America, 95/6, 2081–2092. https://doi.org10.1785/0120050077, 2005.

765   Brocher, T. M.: Compressional and Shear-Wave Velocity versus Depth Relations for Common Rock Types in Northern California, Bulletin of the Seismological Society of America, 98/2, 950–968. doi: 10.1785/0120060403, 2008.

Brückl, E., Bleibinhaus, F., Gosar, A., Grad, M., Guterch, A., Hrubcová, P., Keller, G. R., Majdański, M., Šumanovac, F., Tiira, T., Yliniemi, J., Hegedus, E., and Thybo, H.: Crustal
770   structure due to collisional and escape tectonics in the Eastern Alps region based on profiles Alp01 and Alp02 from the ALP 2002 seismic experiment, Journal of Geophysical Research, 112, B06308, doi:10.1029/2006JB004687, 2007

Cloetingh, S., Bada, G., Matenco, L., Lankreijer, A., Horvath, F., and Dinu, C.: Modes of basin(de)formation, lithospheric strength and vertical motions in the Pannonian–Carpathian
775   system:inferences from thermo-mechanical modeling, Geological Society, London, Memoirs, 32, 207–221, https://doi.org/10.1144/GSL.MEM.2006.032.01.12, 2006

Csontos, L., and Vörös, A.: Mesozoic plate tectonic reconstruction of the Carpathian region, Palaeoclimatology, Palaeoecology, Palaeogeography, 210, 1–56, https://doi.org/10.1016/j.palaeo.2004.02.033, 2004

780   Cvetko Tešović, B., Martinuš, M., Golec, I., and Vlahović, I.: Lithostratigraphy and biostratigraphy of the uppermost Cretaceous to lowermost Palaeogene shallow-marine succession: top of the Adriatic Carbonate Platform at the Likva Cove section (island of Brač, Croatia), Cretaceous Research, 114, 104507, https://doi.org/10.1016/j.cretres.2020.104507, 2020.

785   de Kool, M., Rawlinson, N., and Sambridge. M.: A practical grid-based method for tracking multiple refraction and reflection phases in three-dimensional heterogeneous media. Geophys. J. Int, 167, 253270, doi: 10.1111/j.1365-246X.2006.03078.x, 2006

Dragašević, T., and Andrić, B.: Dosadašnji rezultati ispitivanja građe Zemljine kore dubokim seizmičkim sondiranjem na području Jugoslavije (in Serbian). Acta Seismologica Iugoslavica,
790   2–3, 47–50, 1975.

Fodor, L., Jelen, B., Márton, E., Skaberne, D., Čar, J., and Vrabec, M.: Miocene–Pliocene tectonic evolution of the Slovenian Periadriatic fault: implications of Alpine–Carpathian extrusion models, Tectonics, 17, 690–709, https://doi.org/10.1029/98TC01605, 1998.

Frisch, W., Kuhlemann, J., Dunkl, I., and Brugel, A.: Palinspastic reconstruction and topographic evolution of the Eastern Alps during late Tertiary tectonic extrusion, Tectonophysics, 297, 1–15, https://doi.org/10.1016/S0040-1951(98)00160-7, 1998.

Geological Map of Albania 2002: Geological 1 : 200 000 map published by the Ministry of Industry & Energy and the Ministry of Education & Science, Tirana.

Grad, M., Tiira, T., and ESC Working Group: The Moho depth map of the European Plate. Geophys. J. Int, 176, 279–292, https://doi.org/10.1111/j.1365-246X.2008.03919.x, 2009.

Handy, M. R., Giese, J., Schmid, S. M., Pleuger, J., Spakman, W., Onuzi, K., and Ustaszewski, K.: Coupled crust-mantle response to slab tearing, bending and rollback along the Dinaride–Hellenide orogen, Tectonics, 38, 2803–2828, https://doi.org/10.1029/2019TC005524, 2019.

Herak, M., Herak, D. and Markušić, S. (1996): Revision of the earthquake catalogue and seismicity of Croatia, 1908–1992, Terra Nova, 8, 86–94.

Horváth, F., Bada, G., Szafián, P., Tari, G., Ádám, A., and Cloetingh, S.: Formation and deformation of the Pannonian basin: constraints from observational data, in: European Lithosphere Dynamics, edited by Gee, D.G., Stephenson, R.A. (Eds.), Memoirs, Geological Society, London, 32, 191–206, https://doi.org/10.1144/GSL.MEM.2006.032.01.11, 2006

Kapuralić, J., Šumanovac, F., and Markušić, S.: Crustal structure of the northern Dinarides and southwestern part of the Pannonian basin inferred from local earthquake tomography, Swiss Jour. of Geosc., 112, 181–198, doi: https://doi.org/10.1007/s00015-018-0335-2, 2019

Magrin, A., and Rossi, G.: Deriving a new crustal model of Northern Adria: The Northern Adria crust (NAC) model, Frontiers in Earth Science, 8:89, https://doi.org/10.3389/feart.2020.00089, 2020.

Matenco, L., and Radivojević, D.: On the formation and evolution of the Pannonian Basin: Constraints derived from the structure of the junction area between the Carpathians and Dinarides, Tectonics, 31, TC6007, https://doi.org/10.1029/2012TC003206, 2012.

Mohorovičić, A.: Potres od 8. X. 1909., Godišnje izvješće zagrebačkog meteorološkog opservatorija, 9(4/1), 1–56, 1910.

Molinari, I., and Morelli, A.: EPcrust: a reference crustal model for the European Plate, Geophys. J. Int., 185, 352–364, https://doi.org/10.1111/j.1365-246X.2011.04940.x, 2011

Olea, R. A.: Geostatistics for engineers and Earth scientists, Springer Science + Business Media, New York, 320 pp., ISBN 978-0792385233, 1999.

Orešković, J., Šumanovac, F., and Hegedüs, E.: Crustal structure beneath the Istra peninsula based on receiver function analysis, Geofizika, 28, 247-263, 2011.

Osnovna Geološka Karta SFRJ: Geological maps of former Yugoslavia, 1 : 100.000, Beograd, Savezni Geoloski Zavod.

830   Pebesma, E. J.: "Multivariable geostatistics in R: the gstat package", Computers & Geosciences, 30, 683–691, https://doi.org/10.1016/j.cageo.2004.03.012, 2004.

Rawlinson, N., and Urvoy, M.: Simultaneous inversion of active and passive source datasets for 3-D seismic structure with application to Tasmania, Geophys. Res. Lett., 33, https://doi.org/10.1029/2006GL028105, 2006.

835   Ratschbacher, L., Merle, O., Davy, P., and Cobbold, P. : Lateral extrusion in the Eastern Alps, Part 1: Boundary conditions and experiments scaled for gravity, Tectonics, 10/2, 245–256, https://doi.org/10.1029/90TC02622, 1991a

Ratschbacher, L., Frisch, W., Linzer, H.-G., and Merle, O.: Lateral extrusion in the Eastern Alps, Part 2: Structural analysis, Tectonics, 10, 257–271, https://doi.org/10.1029/90TC02623,
840   1991b

Royden, L. H., and & Horváth, F.: The Pannonian Basin – A study in basin evolution, edited by Royden, L. H., and & Hórvath, F., AAPG Memoirs, 45, The American Association of Petroleum Geologists Tulsa, Oklahoma (USA) & Hungarian Geological Society, Budapest (Hungary), pp. 394, https://doi.org/10.1306/M45474, 1988.

845   Saftić, B., Velić, J., Sztano, O., Juhasz, G,, and Ivković, Ž.: Tertiary subsurface facies, source rocks and hydrocarbon reservoirs in the SW part of the Pannonian Basin (Northern Croatia and South-Western Hungary), Geologia Croatica, 56/1, 101–122, https://doi.org/10.4154/232, 2003.

Schmid, S. M., Bernoulli, D., Fügenschuh, B., Matenco, L., Schefer, S., Schuster, R., Tischler, M.,
850   and Ustaszewski, K.: The Alpine–Carpathian–Dinaridic orogenic system: correlation and evolution of tectonic units, Swiss J. Geosci., 101, 139-183, https://doi.org/10.1007/s00015-008-1247-3, 2008.

Schmid, S. M., Fügenschuh, B., Kounov, A., Matenco, L, Nievergelt, P., Oberhänsli, R., Pleuger, J., Schefer, S., Schuster, R., Tomljenović, B., Ustaszewski, K., and Van Hinsbergen, D. J. J.:
855   Tectonic units of the Alpine collision Zone between Eastern Alps and western Turkey, Gondwana Research, 78, 308-374, https://doi.org/10.1016/j.gr.2019.07.005, 2020.

Skoko, D., Prelogović, E., and Aljinović, B.: Geological structure of the Earth's crust above the Moho discontinuity in Yugoslavia, Geophysical Journal International, 89(1), 379–382, https://doi.org/10.1111/j.1365-246X.1987.tb04434.x, 1987.

860   Snow, A. D., Whitaker, J., Cochran, M., Van den Bossche, J., Mayo, C., Miara I., de Kloe, J., Karney, C., Couwenberg, B., Lostis, G., Dearing, J., Ouzounoudis, G., Filipe, Jurd, B., Gohlke, C., Hoese, D., Itkin, M., May, R., Heitor, Wiedemann, B. M., Little, B., Barker, C., Willoughby, C., Haberthür, D., Popov, E., Holl, G., de Maeyer, J., Ranalli, J., Evers K., and da Costa, M. A.: pyproj4/pyproj: 3.3.0 Release (3.3.0), Zenodo, https://doi.org/10.5281/zenodo.5709037, 2021.

865   Środoń, J., Anczkiewicz, A. A., Dunkl, I., Vlahović, I., Velić, I., Tomljenović, B., Kawiak, T., Banaś, M., and Von Eynatten, H.: Thermal history of the central part of the Karst Dinarides, Croatia: combined application of clay mineralogy and low-T thermochronology, Tectonophysics, 744, 155–176, https://doi.org/10.1016/j.tecto.2018.06.016, 2018.

Stipčević, J., Tkalčić, H., Herak, M., and Markušić, S.: Crustal and uppermost mantle structure
870   beneath the External Dinarides, Croatia, determined from teleseismic receiver functions, Geophys. J. Int., 185, 1103–1119, https://doi.org/10.1111/j.1365-246X.2011.05004.x, 2011.

Stipčević, J., Herak, M., Molinari, I., Dasović, I., Tkalčić, H., and Gosar, A.: Crustal thickness beneath the Dinarides and surrounding areas from receiver functions, Tectonics, 37, https://doi.org/10.1029/2019TC005872, 2020

875   Šumanovac, F.: Lithosphere structure at the contact of the Adriatic microplate and the Pannonian segment based on the gravity modelling, Tectonophysics, 485/1–4, 94–106, https://doi.org/10.1016/j.tecto.2009.12.005, 2010.

Šumanovac, F., Orešković, J., Grad, M., and ALP 2002 Working Group: Crustal structure at the contact of the Dinarides and Pannonian basin based on 2-D seismic and gravity
880   interpretation of the Alp07 profile in the ALP 2002 experiment, Geophys. J. Int., 179, 615–633, https://doi.org/10.1111/j.1365-246X.2009.04288.x, 2009.

Šumanovac, F., Hegedűs, E., Orešković, J., Kolar, S., Kovács, A. C., Dudjak, D., and Kovács, I. J.: Passive seismic experiment and receiver functions analysis to determine crustal structure at the contact of the northern Dinarides and southwestern Pannonian Basin, Geophys. J. Int.,
885   205. 1420–1436, https://doi.org/10.1093/gji/ggw101 , 2016.

Tari, G., Dövényi, P., Dunkl, I., Horváth, F., Lenkey, L., Stefanescu, M., Szafián, P., and Tóth, T.: Litosphere structure of the Pannonian basin derived from seismic, gravity and geothermal data, in: The Mediterranean Basins: Tertiary Extension within the Alpine Orogen, edited by Durand, B., Jolivet, L., Horváth, F., and Séranne, M., Geological Society of London, Special
890   Publications, 156, 215–250, https://doi.org/10.1144/GSL.SP.1999.156.01.12, 1999.

Tišljar, J., Vlahović, I., Velić, I., and Sokač, B.: Carbonate platform megafacies of the Jurassic and Cretaceous deposits of the Karst Dinarides, Geologia Croatica, 55/2, 139–170, 2002.

Tozer, B., Sandwell, D.T., Smith, W. H. F., Olson, C., Beale, J. R., and Wessel, P.: Global bathymetry and topography at 15 arc sec: SRTM15+, Earth and Space Science, 6, 1847–1864, https://doi.org/10.1029/2019EA000658, 2019.

Ustaszewski, K., Schmid, S. M., Fügenschuh, B., Tischler, M., Kissling, E., and Spakman, W.: A map-view restoration of the Alpine–Carpathian–Dinaridic system for Early Miocene, Swiss Jour. of Geosc., 101, Supplement 1, 273–294, https://doi.org/10.1007/s00015-008-1288-7, 2008.

Ustaszewski, K., Schmid, S. M., Lugović, B., Schuster, R., Schlategger, U., Bernoulli, D., Hottinger, L., Kounov, A., Fügenschuh, B., and Schefer, S.: Late Cretaceous intra-oceanic magmatism in the internal Dinarides (northern Bosnia and Herzegovina): Implication for the collision of the Adriatic and European Plates, Lithos, 108, 106–125, https://doi.org/10.1016/j.lithos.2008.09.010, 2009.

Velić, I., Vlahović, I., and Matičec, D.: Depositional sequences and palaeogeography of the Adriatic Carbonate Platform, Mem. Soc. Geol. Ital., 57, 141–151, 2002.

Vlahović, I., Tišljar, J., Velić, I., and Matičec, D.: Evolution of the Adriatic Carbonate Platform: Palaeogeography, main events and depositional dynamics. Palaeogeogr. Palaeoclimatol. Palaeoecol., 220/3–4, 333–360, https://doi.org/10.1016/j.palaeo.2005.01.011, 2005.

895

900

905

910

915

Appendix A

Table A1. Estimation of Carbonate Rock Complex (CRC) bottom depth in Dinarides. CRC bottom depths were estimated based on 93 sheets of Basic Geological Map (1:100,000) of former Yugoslavia (Osnovna Geološka Karta SFRJ) and 1:200,000 Geological Map of Albania (Geological Map of Albania, 2002). The CRC bottom depth values were estimated for each map centroid, in respect to External Dinarides structural relations, deformation styles that incorporate thrusting, folding (e.g., Balling et

925 al., 2021), and thicknesses of deposits on individual maps. Regional nappe systems in External Dinarides incorporate up to six individual structural levels composed of thrust sheets of laterally and/or vertically variable thicknesses, enabling estimated combined absolute CRC depth up to 14,200 m.

No.	Basic Geological Map (BGM)	BGM centroid coordinates		Estimated average elevation	Estimated absolute bedrock depth (m)	Number of structural levels
		Latitude (φ)	Longitude (λ)	(m a.s.l.)		
1	Albania Nord	42.090	20.048	805	8200–14200	2–5
2	Banja Luka	44.834	17.247	300	1200	0–2
3	Bar	42.167	19.243	400	11100	2–4
4	Bihać	44.836	15.742	600	8400	2–3
5	Bijeljina	44.831	19.245	-	Saftić et al. (2003)	-
6	Biograd	43.830	15.244	-40	7900	1–2
7	Biševo	42.833	16.243	-70	7600	1–2
8	Bosanska Krupa	44.832	16.247	400	3700	0–2
9	Bosanski Novi	45.165	16.242	200	200	0

10	Brčko	44.831	18.739	-	Saftić et al. (2003)	-
11	Budva	42.167	18.747	-100	9100	2–4
12	Bugojno	44.160	17.233	900	6500	1–3
13	Cres	44.836	14.249	0	7200	1–2
14	Crikvenica	45.171	14.741	400	8300	2–3
15	Črnomelj	45.504	15.251	350	8200	1–2
16	Delnice	45.504	14.739	600	7900	1–2
17	Derventa	44.832	17.740	250	200	0–1
18	Doboj	44.837	18.246	-	Saftić et al. (2003)	-
19	Drniš	43.832	16.251	500	9000	2–3
20	Drvar	44.499	16.240	700	7800	2–3
21	Dubrovnik	42.497	18.244	200	9000	2–3
22	Foča	43.499	18.754	1000	300	0–1
23	Gacko	43.166	18.746	1300	10400	1–5
24	Glamoč	44.168	16.746	1000	8500	2–3
25	Gorica	45.830	13.747	350	7400	2–3
26	Gospić	44.496	15.247	500	10400	3–4
27	Ilirska	45.502	14.240	400	7900	2–3

	Bistrica					
28	Imotski	43.502	17.246	800	13000	2–4
29	Jabuka	43.164	15.266	-150	7700	1–2
30	Jajce	44.492	17.246	600	4100	1–3
31	Jelsa	43.169	16.742	0	8900	1–2
32	Kalinovik	43.496	18.247	900	9000	1–4
33	Karlovac	45.502	15.750	200	1000	0–2
34	Ključ	44.501	16.743	700	7500	2–3
35	Knin	44.166	16.246	550	9500	2–3
36	Korčula	42.836	17.246	-50	6600	1–2
37	Kostajnica	45.167	16.751	250	200	0
38	Kotor	42.500	18.743	700	10300	2–5
39	Kranj	46.158	14.141	700	6800.00	2–3
40	Labin	45.169	14.245	300	6500	1–2
41	Lastovo	42.836	16.745	-80	8100	1–2
42	Livno	43.835	17.246	1100	11200	2–4
43	Lošinj	44.503	14.241	0	6200	1–2
44	Ljubovija	44.147	19.245	500	100	0–1

45	Metković	43.167	17.750	250	13100	3–4
46	Molat	44.163	14.745	-50	7200	1–2
47	Mostar	43.500	17.740	900	13500	4–5
48	Nevesinje	43.163	18.242	1000	14100	4–5
49	Nikšić	42.833	18.750	1000	12600	5–6
50	Nova Gradiška	45.167	17.247	-	Saftić et al. (2003)	-
51	Nova Kapela	45.165	17.743	-	Saftić et al. (2003)	-
52	Novo Mesto	45.837	15.240	250	7300	1–2
53	Obrovac	44.170	15.746	300	10000	2–3
54	Ogulin	45.171	15.250	400	9400	2–3
55	Omiš	43.502	16.751	450	10200	2–4
56	Otočac	44.829	15.248	500	10200	3–4
57	Ploče	43.169	17.246	250	10500	2–4
58	Pljevija	43.490	19.261	1000	200	0–1
59	Postojna	45.835	14.249	700	7700.00	2–3
60	Prača	43.814	18.749	1000	0	0–1
61	Prijedor	44.834	16.741	400	2400	0–2

62	Primošten	43.504	15.750	-100	7600	1–2
63	Prozor	43.824	17.743	1100	7500	0–4
64	Pula	44.831	13.743	0	4600	1
65	Rab	44.829	14.742	100	9200	2–3
66	Ribnica	45.837	14.751	600	7200	1–2
67	Rovinj	45.165	13.749	20	4500	1
68	Sarajevo	43.829	18.253	700	2600	1–3
69	Šavnik	42.833	19.252	1000	10600	1–5
70	Šibenik	43.837	15.741	50	8000	2–3
71	Silba	44.496	14.744	0	8000	2–3
72	Sinj	43.835	16.749	800	12000	3–4
73	Slavonski Brod	45.170	18.239	-	Saftić et al. (2003)	-
74	Slunj	45.169	15.746	350	4500	0–2
75	Split	43.500	16.244	100	7500	1–2
76	Ston	42.834	17.748	200	9000	1–3
77	Svetac	43.171	15.746	-150	7700	1–2
78	Teslić	44.491	17.736	700	700	0–3

79	Titograd	42.500	19.253	700	12200	4–5
80	Tolmin	46.153	13.610	700	6600.00	2–3
81	Trebinje	42.830	18.249	700	12000	2–4
82	Trst	45.497	13.741	200	6000	2–3
83	Tuzla	44.489	18.742	400	300	0–1
84	Udbina	44.503	15.750	800	12000	3–4
85	Ulcinj	41.825	19.244	-200	9200	2–3
86	Vareš	44.144	18.245	800	1600	0–1
87	Vis	43.166	16.250	–70	7600	1–2
88	Višegrad	43.813	19.271	700	700	0–1
89	Vlasenica	44.147	18.745	600	700	0–1
90	Žabljak	43.166	19.250	1200	2400	1–5
91	Zadar	44.163	15.245	10	8000	2–3
92	Zavidovići	44.495	18.252	350	0	0
93	Zenica	44.149	17.733	800	1200	0–3
94	Zvornik	44.489	19.245	250	800	0–1

930

Appendix B

Input data point locations

The following figure shows the exact location of data points used for interpolation of model interfaces and parameters. Data points used for each interface and parameter are shown in a separate figure panel.
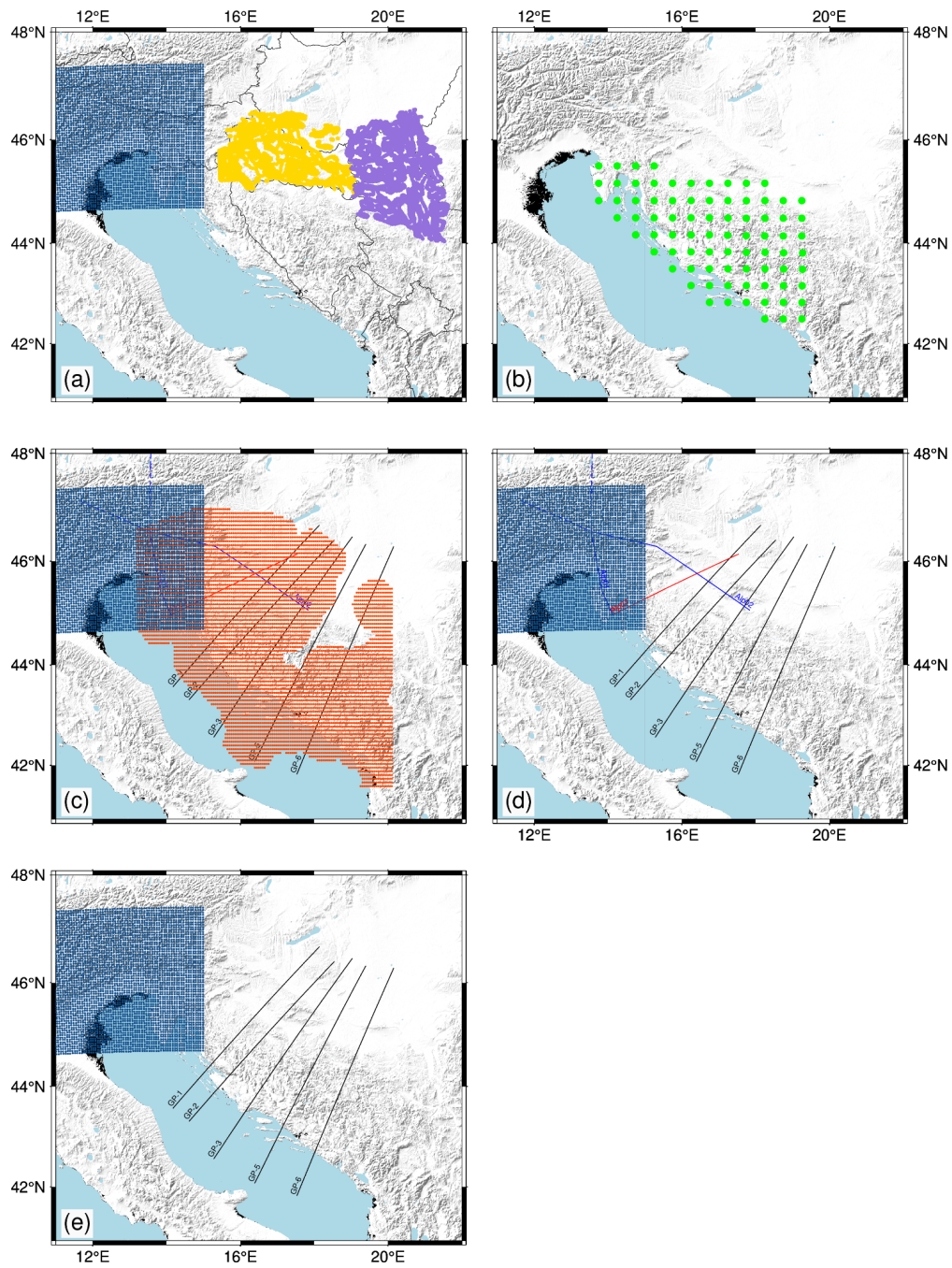
Fig. B1 Point locations of data used for interpolation of (a) sediment bottom depth, (b) CRC depth, (c) Moho depth, (d) P-wave velocity, (e) density. Yellow points mark data from Saftić et al. (2003), purple points mark data from Matenco & Radivojević (2012), green points mark data on CRC depths, blue points mark data from the NAC model (Magrin & Rossi, 2020), orange points mark data from Stipčević et al. (2011), blue lines mark the positions of profiles from Brückl et al. (2007), red lines mark the profile from Šumanovac et al. (2009), and black lines mark the gravimetric profiles from Šumanovac (2010).

Appendix C

Kriging

Kriging is a method of interpolation formulated for the estimation of a continuous spatial attribute (e.g. depth to Moho interface) at an unknown site, using the limited set of data from sampled sites. It is a form of generalized linear regression used for the formulation of an optimal estimator in a minimum mean square error sense (Olea, 1999).

Generally, the value at a point of interest is calculated as follows:

$$\hat{Z}(x_0) = \sum_{i=1}^{n} \lambda_i Z(x_i),$$

where $\hat{Z}(x_0)$ is value estimation at point of interest x_o, λ_i are weights, and $Z(x_i)$ are known values at sites x_i. The kriging weights are derived from the covariance of the sampled values. The first step in kriging interpolation is estimation of the variogram (also called a semivariogram) – a statistic that assesses the average decrease in similarity between two random variables as the distance between them increases. It is the inverse of covariance – the covariance measures similarity, and the variogram measures dissimilarity. Unlike the other moments (e.g., the mean), the variogram is not a single number, but a continuous function of a variable h, called the lag. The variogram calculated from the sampled points is called the experimental variogram. The experimental variogram is not used in the calculation of kriging weights but is used to fit a theoretical variogram which in turn is used for calculation of the weights. When fitting, we can use limited types of semivariograms which have acceptable properties needed for solving the system of equations in order to obtain the weights. If we would use the experimental variogram directly, we might end up with an unsolvable system of equations. For example, **Fig. A1** shows an experimental and theoretical variogram used for interpolation of Moho interface depth. A variogram, such as the one in **Fig. A1**, that increases in dissimilarity with distance over short lags and then levels off is called a transitive variogram. The lag at which it reaches a constant value is called the range, and that constant value is called the sill. For the Moho depth interpolation, we had an abundance of data available, and we were able to estimate a theoretical variogram which fits the observed data almost perfectly.
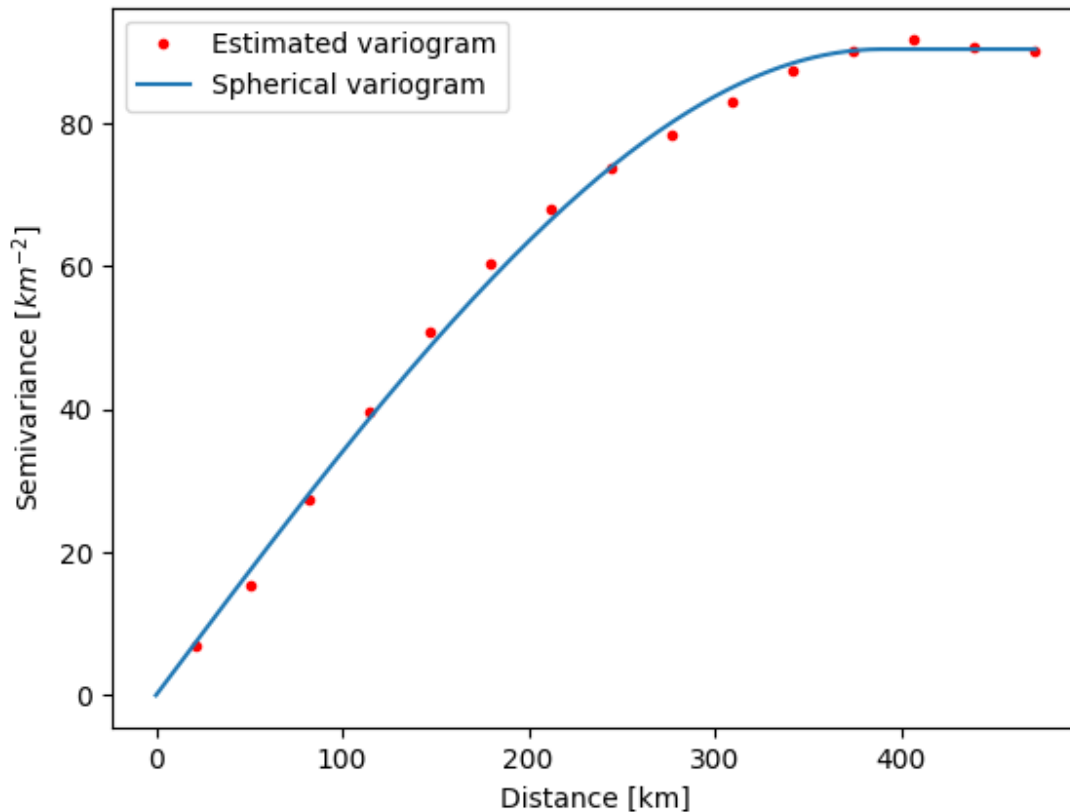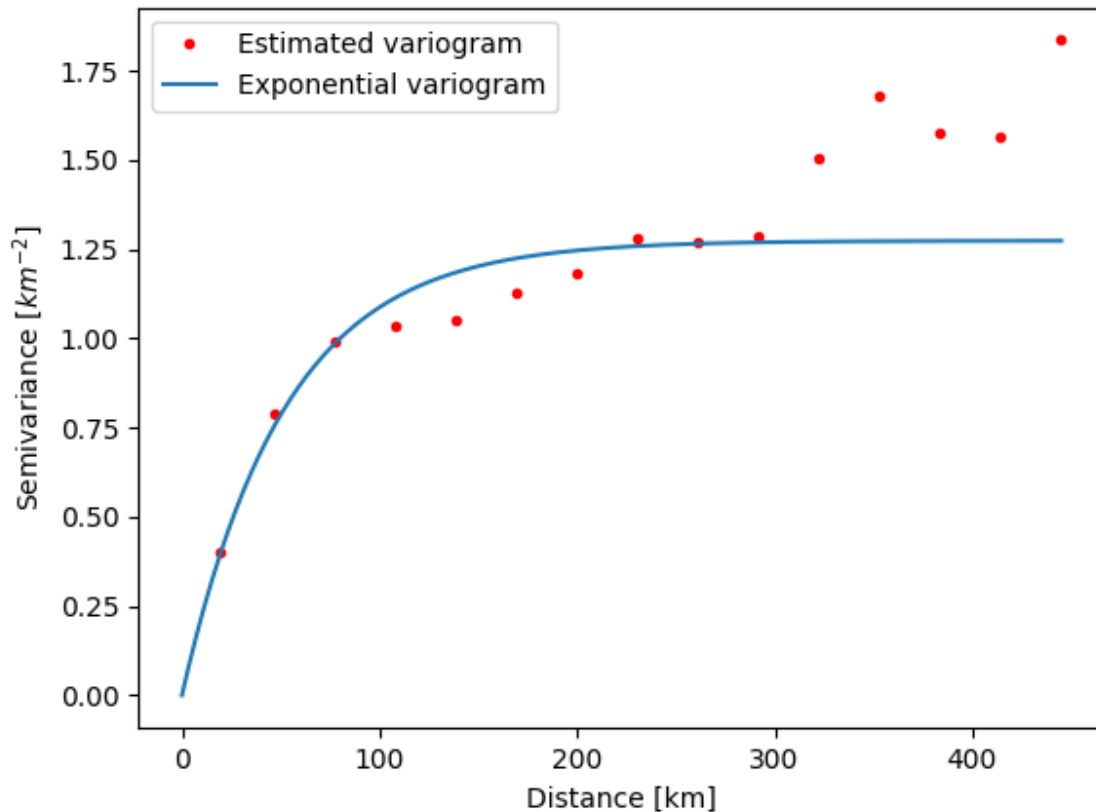
Fig. C1. Estimated and theoretical (spherical) variogram used for interpolation of Moho interface depth.

980　　In case of other model parameters, we did not have such a perfect fit for larger lags. For instance, **Fig. C2** shows the variogram used for Neogene deposits bottom interpolation. In this case, the theoretical variogram was not spherical, but exponential. In this case, for the largest lags shown, the theoretical and estimated variograms do not fit. For the calculation of the variogram pairs of measured values are used. Since for the greater distances (greater

985　　lags) there are fewer numbers of such pairs, the estimates are less accurate for those lags. Fortunately, for practical use in kriging, the variogram closer to the origin requires the most accurate estimation (Olea, 1999), and we had that condition met for all our model parameters.

Fig. C2. Neogene deposits bottom estimated and theoretical (exponential) variograms.

Variograms for CRC bottom depth and velocity estimation are shown in **Figs. C3** and **C4,** respectively. Crust velocity variogram shown in **Fig. C4**. is required to have a constant mean in the sample space in order to be able to estimate a variogram. In case of a gentle and systematic variation in the mean (called the drift), e.g. velocity increases with depth, it has to be removed prior to the estimation of the variogram. Such a drift was indeed observed and was removed prior to the estimation of the variogram shown in **Fig. C4**. Besides the drift, we estimated the experimental variogram in several directions, in order to check if it was dependent on the direction (i.e. if there was anisotropy), but we have not observed any anisotropy.
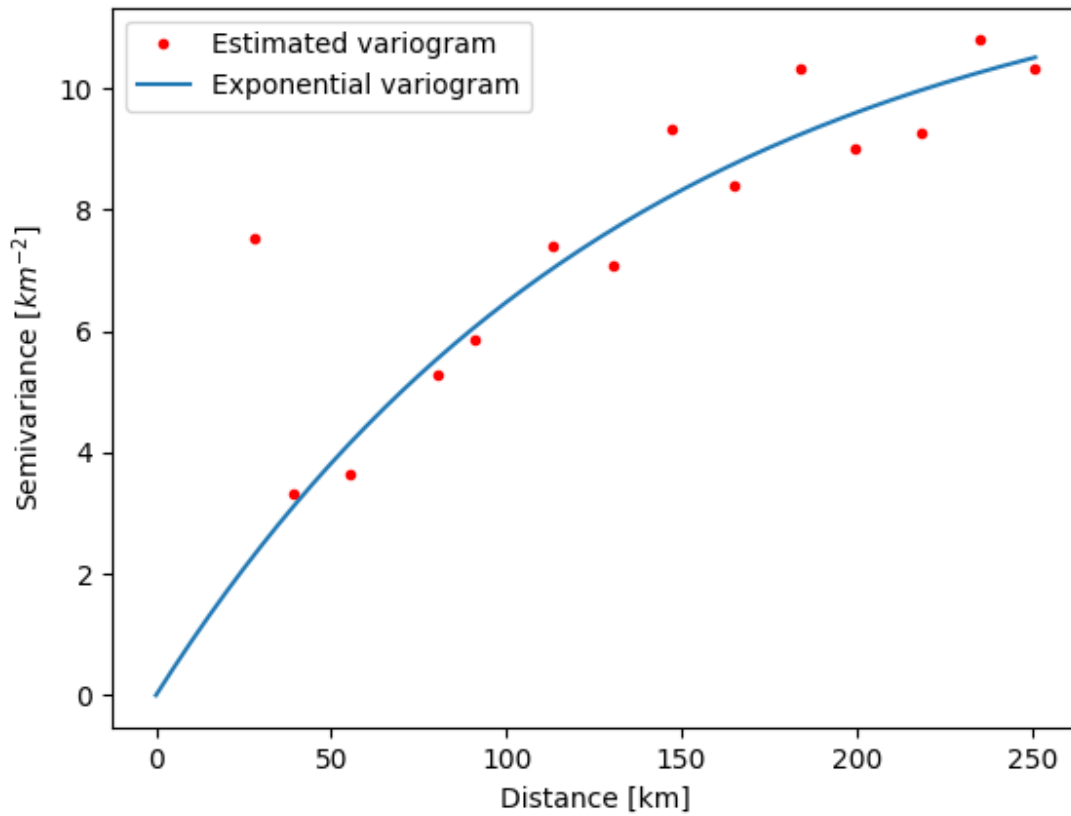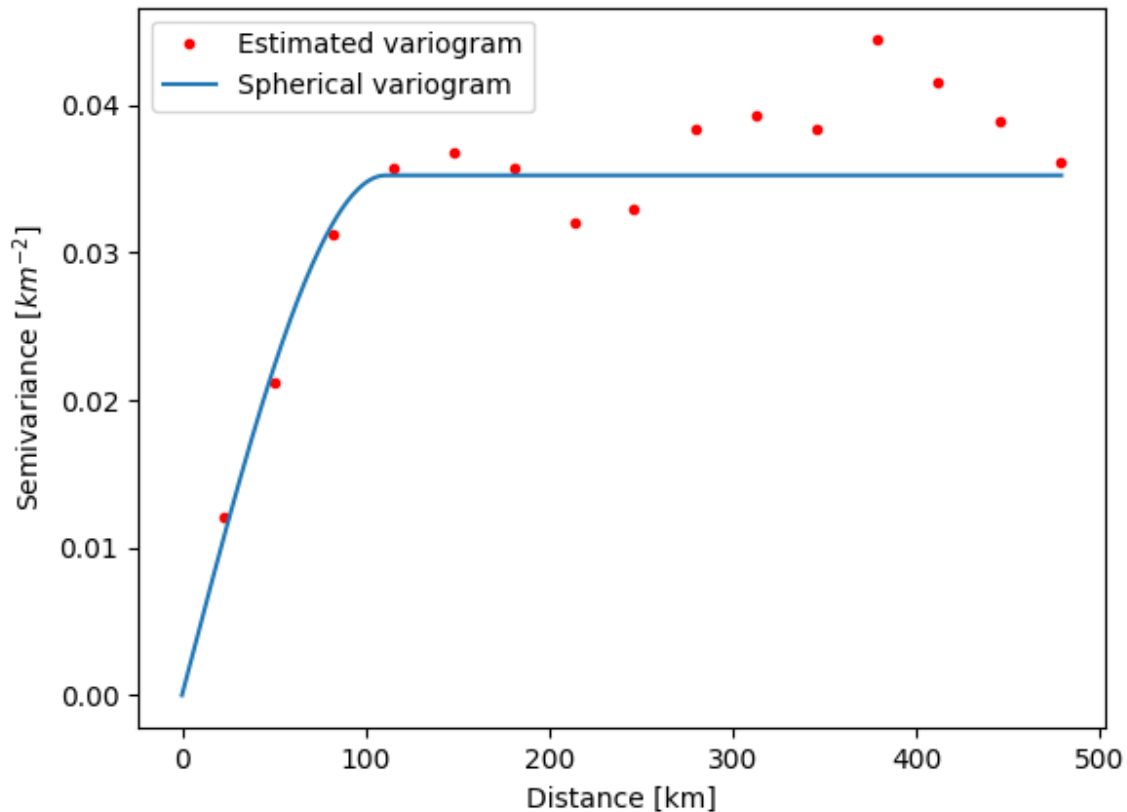
Fig C3. Carbonate Rock Complex (CRC) bottom estimated and theoretical (exponential) variogram.

**Fig. C4.** Estimated and theoretical (spherical) variogram used for interpolation of the crustal velocity (Vp).

Once we had variograms estimated, we were able to obtain the weights and calculate the values of parameters (Moho, Neogene deposits bottom, CRC bottom, velocity) for each point in our grid. All of the operations, both variogram estimation and the interpolation itself, were done using the gstat package (Pebesma, 2004). Alongside the interpolated values, the package also returns the variance estimates for each point in the grid.

The interface parameters (Moho, Neogene deposits bottom and CRC bottom depth) were interpolated using ordinary kriging. Ordinary kriging assumes that the mean of the value is unknown, but constant. For interpolation of the velocity, we had to use a more general type of kriging – the universal kriging. It relaxes the condition on the mean – it is no longer assumed constant. The other properties of kriging are shared between both types used. They are both minimum square error estimates. The estimation is not limited to the data interval (it is possible to extrapolate – although it is less accurate). They have, so called, declustering ability – the measurements that are spatially clustered have lower weights than isolated points. They are exact interpolators with zero kriging variance – meaning that if, for instance, we try to calculate the value exactly at a sampled point, kriging will return the exact value

and assign 0 variance to it. It can be nicely seen in **Fig. 5** showing the velocity variances. Since
1025   the variance at sampled sites is zero it is possible to discern the profiles that were sampled for data. Kriging is not able to handle duplicate points – it causes the insolvable systems of equations for the kriging weights – therefore we had to handle such points. It is also worth mentioning that the variance returned by the kriging software does not depend on variance or values of individual observations, but only on the sampling pattern. Therefore, we added
1030   the (estimated or available) data variance to the variance obtained from the kriging and called it the total variance.

Appendix D

Comparison of the new model to existing regional models
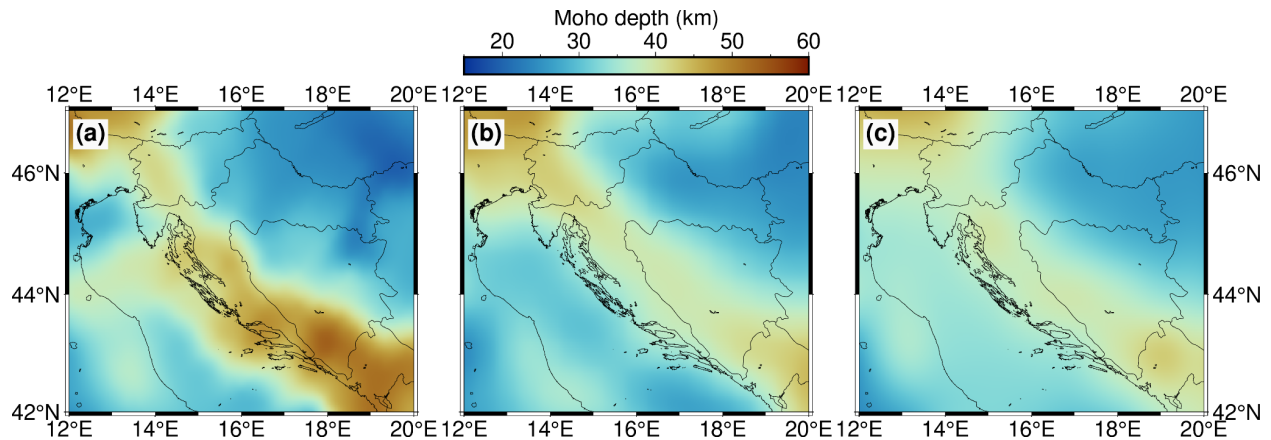
Fig. D1 Comparison of Moho depths among (a) our newly derived model, (b) Grad et al. (2009) european Moho model, and (c) EPcrust model (Molinari and Morelli, 2011).

Compared to existing regional models, Moho depth is considerably greater in the new model, especially in the southern part of the Dinarides.

The EPcrust model has sediment bottom depth defined. In our model, we discern CRC bottom and Neogene sediment bottom, which is not defined separately in the (regional) EPcrust model. Therefore, we put both of them in Fig. D2.
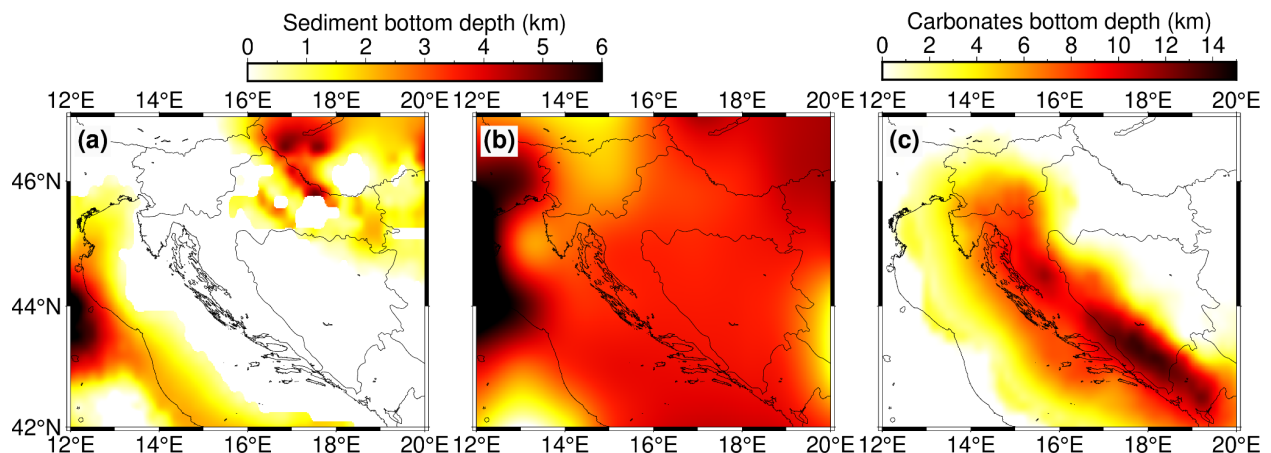

Fig. D2 Comparison of sediment bottom depth as defined as (a) Neogene sediment bottom depth in our model, (b) sediment bottom in EPcrust model, and (c) CRC bottom depth in our model.

The horizontal variations in sediment and CRC bottom depths are much more pronounced than in the regional EPcrust model.

53

In the EPcrust model, the velocity is defined as two layers (upper and lower crust) with constant velocity value (for a given grid point, it does not vary with depth; it varies horizontally, though). Therefore, we have picked two depths in our model, since we defined velocity as varying in all three dimensions. Even though we do not define crust as two layers (lower or upper crust), we have picked velocity at depth of 15 km to compare with EPcrust upper crust, and velocity at depth of 25 km to compare with EPcrust lower crust. The comparison is shown in Fig. D3.
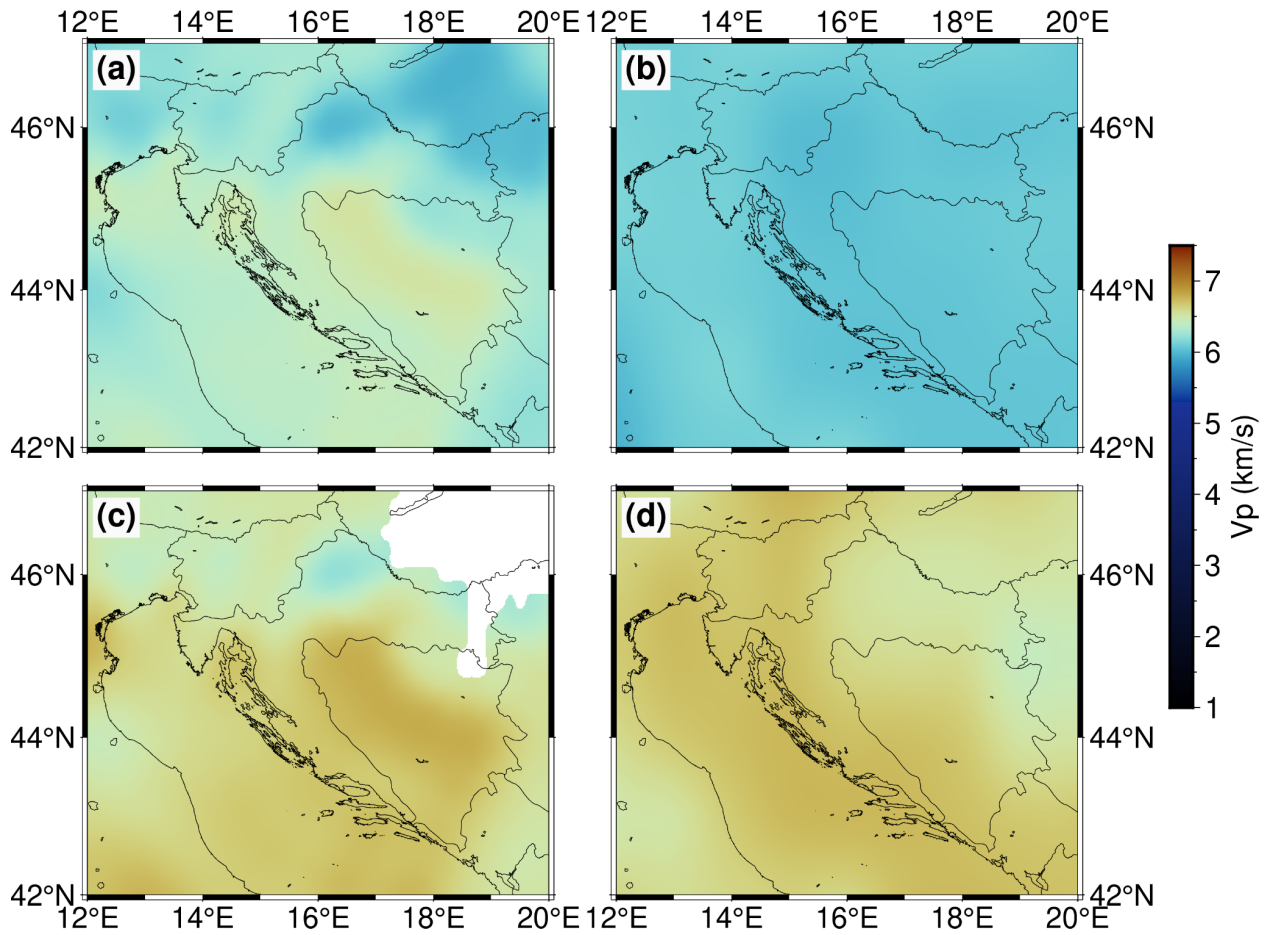
Fig. D3 Comparison of P-wave velocity: (a) our model at 15 km depth, (b) EPcrust upper crust, (c) our model at 25 km depth, (d) EPcrust lower crust.

There is noticeable horizontal variation of velocity values in our model compared to the velocities defined in the EPcrust model, due to inclusion of data from refraction and gravimetric profiles.